Construction and Building Materials 521 (2026) 146166

Contents lists available at ScienceDirect

Construction and Building Materials

journal homepage: www.elsevier.com/locate/conbuildmat

Sodium sulfate, silicate, or carbonate? Activator-specific pathways, kinetics, and strength development in ultra-low-clinker hybrid binders

Hania Miraki [a,c,*], Maciej Zajac [a], Mohsen Ben Haha [a], Arnaud Muller [a], Klaartje de Weerdt [b], Ravi Patel [c], Frank Dehn [c]

[a] Heidelberg Materials AG, Global R&D, Oberklamweg 2-4, Leimen 69181, Germany
[b] Norwegian University of Science and Technology (NTNU), Materialteknisk, 3-230, Gløshaugen, Richard Birkelands vei 1a, Trondheim, Norway
[c] Institute for Concrete Structures and Building Materials (IMB/MPA/CMM), Karlsruhe Institute of Technology (KIT), Gotthard-Franz-Str. 3, Karlsruhe 76131, Germany

ARTICLE INFO

Keywords:
Low-clinker systems
Hybrid binders
Alkali activation
Hydration mechanism
Ettringite formation
Porosity

ABSTRACT

This study investigates hybrid binders (25% Portland cement, 50% calcined clay, 25% limestone) activated with sodium sulfate, sodium carbonate, and sodium metasilicate at different alkali levels. Mechanical performance, hydration kinetics, and microstructure were evaluated using a multi-technique approach. Sodium sulfate at 1.5% Na_2O_{eq} achieved the highest early strength with only a minor reduction at 28 days and was associated with stable ettringite formation. This performance was sensitive to mixing conditions, as the use of $Na_2SO_4{\cdot}10H_2O$ required controlled storage to avoid pre hydration of the cement. In contrast, ettringite formation was suppressed in both sodium carbonate and sodium metasilicate hybrid binders despite having the total same sulfate content with the references. Sodium metasilicate accelerated hydration and was characterized by the formation of Na-substituted AFm (U-phase). Sodium carbonate system was characterised by limited carbonate-AFm formation detected only in fresh samples, with no persistence after hydration stoppage. Porosity analysis showed that, unlike the reference systems, the hybrid binders developed strength with hydration time without substantial refinement or redistribution of the coarser part of the MIP-accessible pore network. Sodium metasilicate hybrid binder exhibited H_2O-BET values comparable to sodium sulfate activation and a smaller critical pore diameter yet developed substantially lower compressive strength. Sodium carbonate hybrid binder showed the smallest critical pore diameter among all systems but significantly lower strength. These results demonstrate that in these hybrid binders, porosity refinement, critical pore diameter, and accessible surface area are not sufficient descriptors to explain strength development, challenging a common assumption in blended cement systems.

1. Introduction

Concrete is the most widely used construction material worldwide, with Portland cement acting as its primary binder. Reducing the clinker content of cement is a key strategy for lowering associated CO_2 emissions [1]. In current practice, this is mainly achieved through composite cements, in which Portland clinker is partially replaced by supplementary cementitious materials (SCMs) such as blast furnace slag and fly ash. However, the availability of these conventional SCMs is decreasing due to changes in steel production and the phase-out of coal-fired power plants. Calcined clay has therefore emerged as a widely available alternative SCM.

To further reduce clinker content, some studies have investigated fully clinker-free binder systems, such as geopolymers based on aluminosilicate-rich precursors. In these systems, adequate early-age strength is commonly achieved using highly alkaline activating solutions, often based on concentrated alkali hydroxides or alkali silicates. Reported formulations typically involve high-molarity alkali hydroxide solutions, for example NaOH concentrations in the range of 8–10 M [2,3]. Such activation conditions introduce challenges related to handling, safety, and cost, which have limited their broader application in conventional cementitious systems.

An alternative approach explored in the literature involves binders containing a limited fraction of Portland clinker, typically below 30 wt

* Corresponding author at: Heidelberg Materials AG, Global R&D, Oberklamweg 2-4, Leimen 69181, Germany.
E-mail addresses: hania.miraki@heidelbergmaterials.com, hania.miraki@student.kit.edu (H. Miraki), maciej.zajac@heidelbergmaterials.com (M. Zajac), mohsen.benhaha@gmail.com (M. Ben Haha), arnaud.muller@heidelbergmaterials.com (A. Muller), klaartje.d.weerdt@ntnu.no (K. de Weerdt), ravi.patel@kit.edu (R. Patel), frank.dehn@kit.edu (F. Dehn).

https://doi.org/10.1016/j.conbuildmat.2026.146166
Received 10 January 2026; Received in revised form 24 March 2026; Accepted 26 March 2026
Available online 30 March 2026

%, combined with predominantly aluminosilicate supplementary cementitious materials, so-called hybrid binders. In these systems, clinker hydration contributes to early-age strength development, allowing early performance to be achieved with substantially lower alkaline activator contents. This formulation avoids reliance on high alkali dosages while enabling further clinker reduction compared to conventional composite cements; however, systematic investigations of such extremely low-clinker systems remain limited.

Hybrid systems have been reported in the literature to exhibit the formation of distinct calcium–aluminosilicate–hydrate (C–A–S–H) and sodium–aluminosilicate–hydrate (N–A–S–H) type gels, which complicate the analysis of the resulting binder structure [4,5]. The properties of these low-calcium systems cannot be directly inferred from the behavior of the individual starting materials. Instead, previous studies suggest that interactions between the calcium source, aluminosilicate source, and alkaline activator play an important role in controlling calcium availability and, consequently, the performance of the binder [6]. One approach to addressing the complexity of hybrid binders is to examine the role of alkali activators in these systems. Understanding how alkalis influence hydration kinetics and phase development can provide insight into the mechanisms governing early-age strength development and microstructural evolution.

The enhancement of early-age strength by the addition of alkalis in cementitious systems has been widely attributed to the acceleration of hydration, particularly of the alite phase. Kumar et al. [7] reported that the addition of sodium and potassium hydroxides increases the pH of the pore solution, thereby accelerating the hydration rate and shortening the induction, acceleration, and deceleration periods. This acceleration is further supported by earlier portlandite precipitation, consistent with a dissolution-controlled mechanism. Mota et al. [8] showed that adding NaOH (1.45 M) almost eliminated the induction period in alite hydration, while combining alkali with gypsum further increased the degree of hydration. Later, Mota et al. [9] extended this work to white Portland cement, finding that both NaOH (1.45 M) and Na_2SO_4 (0.725 M) accelerated early hydration but had contrasting long-term effects: Na_2SO_4 resulted in compressive strengths comparable to the alkali-free system at a given degree of hydration, whereas NaOH led to lower strengths due to a reduced total volume of hydrates, particularly ettringite. To broaden the understanding of alkali addition beyond pure clinker systems, Mota et al. [10] also examined white cement–slag blends (30% cement, 70% slag) activated with NaOH (1.45 M) or Na_2SO_4 (0.725 M). Both activators accelerated the degree of hydration of cement and the degree of reaction of slag at early ages, with a more pronounced effect observed in the presence of NaOH. At later ages, both Na_2SO_4 and NaOH reduced the degree of hydration of cement, with values remaining closer to the alkali-free system for Na_2SO_4 and significantly lower for NaOH; similarly, Na_2SO_4 maintained or increased slag reaction depending on slag type, whereas NaOH significantly reduced slag reaction.

Extending this concept to other blended systems, Fu et al. [11] investigated a 50:50 OPC–slag binder activated with Na_2SO_4, Na_2SiO_3 and NaOH. They reported that Na_2SO_4 increased 1-day strength by approximately 43% due to accelerated alite hydration and increased slag dissolution, linked to higher ionic strength, lower Ca^{2+} activity, and enhanced ettringite formation. The activators were compared both at matched alkali contents and at their respective applied dosages. For the alkali-equivalent comparison, Na_2SO_4 was evaluated against Na_2SiO_3 and NaOH at Na_2O_{eq} levels corresponding to the Na_2O supplied by 1% and 2.5% Na_2SO_4. Under these matched alkali conditions, Na_2SO_4 produced the highest 28-day compressive strength. In contrast, when the activators were compared at their actual applied dosages (Na_2SO_4 at its tested levels and Na_2SiO_3 at 1 wt%), the 1% Na_2SiO_3 system achieved the highest 28-day strength among the activated mixtures.

To support the shift toward lower-clinker formulations, Etcheverry et al. [12] investigated hybrid binders with 70% GGBFS and 30% Portland cement activated by Na_2SO_4 (0–15 wt% of slag, optimum = 8%), showing that Na_2SO_4 significantly accelerated hydration kinetics, shortened setting times, and improved early strength by up to threefold at 2 days, with calorimetry and ultrasonic measurements confirming faster stiffening and MIP revealing pore refinement. Further, Etcheverry et al. [13] showed that Na_2SO_4 accelerates hydration and increases early ettringite formation in GGBFS–PC blends, while the main reaction product in both activated and non-activated systems remains a C-(A)-S-H gel. ^{29}Si MAS NMR revealed a more pronounced $Q^2(1Al)$ resonance in the activated system, indicating greater Al incorporation into the C-(A)-S-H chains. XRD and DTG further demonstrated that Na_2SO_4 promotes more AFt (ettringite) and suppresses AFm phases yet does not alter the fundamental C-(A)-S-H gel structure.

Comparable trends have been observed in LC^3 systems. Hanpongpun and Scrivener [14] increased the alkali content of LC^3-65 by adding KOH, raising the Na_2O_{eq} from 0.44% to 1.21%. This modification accelerated clinker hydration and improved early-age strength, with 1-day strength increasing from 13 MPa to 16 MPa. However, the higher alkali level also led to reduced carboaluminate formation and lower strength development at later ages. Recent studies on white Portland cement suggest that this strength reduction is due to faster internal drying, limited pore saturation, and a lower degree of hydration at later ages [15]. Beyond hydroxides, other activators have shown promise. Dai et al. [16] showed that adding a small, optimized dose of sodium silicate (≈1 wt% Na_2O, silicate modulus ≈0.4) to LC^3 significantly improves early-age performance. The activator reduced yield stress and enhanced flowability, while accelerating clinker hydration and synergistic reactions with calcined clay and limestone. This led to up to 120% higher 1-day strength compared to LC^3 and a refined pore structure without compromising 28-day strength. In contrast, increasing the silicate modulus slows hydration and reduces strength development, while raising the alkali content to 2.5 wt% Na_2O additionally triggers U-phase formation, which further compromises long-term strength.

While most studies on alkali activation have focused on systems with moderate clinker contents, extremely low-clinker binders present unique challenges. In such systems, the limited availability of portlandite and the high alumina content of SCMs strongly influence reaction kinetics and phase assemblage, making early strength development particularly challenging. Sun et al. [17] showed that when clinker content drops below 50%, the metakaolin reaction becomes increasingly limited by the rapid depletion of portlandite (CH), leading to reduced strength development, particularly after the first few days. Adding portlandite restored its availability, enhanced metakaolin reaction and carboaluminate formation, and improved later-age strength, although this came at the cost of a higher CO_2 footprint. Complementary microstructural evidence from Zunino and Scrivener [18] showed that although LC^3-35 and LC^3-25 develop a compact microstructure with substantial hemicarboaluminate and monocarboaluminate precipitation, their early-age (1–2 day) strength remains distinctly lower than PC due to their reduced clinker content. Nevertheless, both LC^3 systems met the 7-day and 28-day strength classes used as the benchmark in their study, while highlighting that early-age reactivity remains a key limitation in low-clinker LC^3 formulations.

Because class F fly ash is a low-calcium aluminosilicate SCM [19], which is closer in chemistry to calcined clays than slag, mechanistic and performance insights from high-volume fly ash hybrid cements are particularly relevant when discussing activator effects in low calcium hybrid systems. In this context, García-Lodeiro et al. [20] proposed a descriptive hydration model for hybrid alkaline fly ash cements typically formulated with ~70–80 wt% fly ash and ~20–30 wt% clinker. Their key point is that these binders do not behave as a simple superposition of "diluted Portland cement hydration" and "separately activated fly ash"; rather, hydration involves the concurrent development of calcium-bearing hydrate assemblages associated with clinker and alkali aluminosilicate-type reaction products controlling the evolving gel chemistry.

The need for acceleration in extremely low-clinker systems also

aligns with evidence from other hybrid binders, where activator chemistry has been shown to strongly influence hydration pathways and early strength. Donatello et al. [21] studied a hybrid cement with ~80 wt% fly ash and ~20 wt% clinker activated by 4% Na_2SO_4. Addition of Na_2SO_4 accelerated alite hydration, shortened setting time, and improved early strength compared to a reference gypsum, while limiting ettringite formation. Alahrache et al. [22] studied a hybrid binder composed of 70 wt% siliceous fly ash and 30 wt% Portland cement, activated with (K, Na)$_2SiO_3$, Na_2CO_3, Na_2-oxalate, and K_3-citrate. The addition of Na_2-oxalate and (K,Na)$_2SiO_3$ significantly accelerated setting and improved early-age compressive strength, while high alkali concentrations were associated with reduced strength at later ages. Thermodynamic modeling indicated that elevated pH and ionic strength in the pore solution contributed to partial destabilization of ettringite, and XRD/TGA analyses showed lower ettringite content at 28 days in systems with higher alkali and aluminum concentrations, where increased aluminum uptake by C-S-H was expected.

García-Lodeiro et al. [5] investigated the early hydration kinetics of hybrid binders containing 30 wt% Portland cement and 70 wt% fly ash, comparing activation with NaOH + Na_2SiO_3 (pH ≈ 13.25) and Na_2CO_3 (pH ≈ 11.6). The authors reported that the type of activator significantly affected hydration kinetics and secondary phase formation. In both systems, the main reaction products were identified as mixtures of C–A–S–H and (N,C)–A–S–H gels, reflecting the interaction between clinker hydration and alkali activation of the aluminosilicate precursor.

Similarly, Xue et al. [4] examined hybrid alkali-activated binders containing 25 wt% Portland cement and 75 wt% supplementary precursors, activated with NaOH and sodium silicate (3–5% Na_2O equivalent). They reported that systems with the highest fly ash content exhibited slower hydration kinetics due to the lower intrinsic reactivity of fly ash. However, microstructural analyses indicated the formation of a cementitious matrix composed mainly of C-(A)-S-H and N-A-S-H gels, and the authors observed that increasing the alkali dosage enhanced the reaction extent and compressive strength in these low-clinker hybrid systems.

Barboza-Chávez et al. [23] also highlight the relevance of combining fly ash with metakaolin within low-clinker hybrid concepts. In their work, hybrid cements containing 20% clinker and varying proportions of fly ash and metakaolin were activated using a mixture of sodium silicate and NaOH corresponding to a very high alkali content of approximately 16–18% Na_2Oeq relative to the binder. The authors reported that, under these alkaline conditions, the binders achieved mechanical performance comparable to an OPC reference. They also reported the formation of a dense matrix with gel chemistries consistent with calcium-bearing hydrates and alkali aluminosilicate-type reaction products, indicating the coexistence of clinker hydration and alkali activation processes.

In parallel, Joseph et al. [24] investigated the chemical activation of hybrid low-clinker binders, in which Portland cement was partially replaced by high volumes of fly ash, focusing mainly on mixtures containing 50 wt% fly ash and 50 wt% cement, with additional systems reaching 60 wt% fly ash replacement. In non-activated blends, increasing fly ash content reduced compressive strength due to the low reactivity of fly ash, with the 50% FA mixture reaching about 33 MPa at 28 days compared with about 62 MPa for OPC. However, activation with Na_2SO_4 solutions (0.75–0.98 M) significantly enhanced the reactivity of the system, increasing the 28-day strength of the 50% FA blend to approximately 64–66 MPa, comparable to the OPC reference. Even at 60% fly ash replacement, Na_2SO_4 activation resulted in strengths around 52 MPa at 28 days.The improvement was associated with higher bound water content, pore refinement, and changes in hydration products, including reduced portlandite and AFm phases together with increased ettringite formation.

Beyond composition alone, activator addition methods for solid salts have also been investigated. Fernández-Jiménez et al. [25] studied binders containing 50% wt% fly ash with 50% wt% cement activated with Na_2SO_4, explicitly comparing Na_2SO_4 added dissolved in the mixing water versus ground in solid form with the fly ash. While both methods resulted in similar long-term performance, the solid-state addition led to slightly higher early strength.

Despite growing interest in clinker reduction, research on ultra-low calcium and hybrid binder systems remains limited. Most existing studies focus on systems with moderate clinker content, while ultra-low clinker systems i.e., those with less than 30% clinker have not been thoroughly investigated. Moreover, the influence of different alkali types at equivalent alkali levels, and the effect of varying alkali contents, are not well understood. The influence of method of alkali incorporation, whether dry-mixed or pre-dissolved, also remains an underexplored variable, despite its potential impact on hydration kinetics and strength development. Additionally, few studies have integrated mechanical performance with detailed microstructural characterization, leaving a gap in understanding the mechanisms governing strength evolution in these systems.

This study investigates the performance and hydration behavior of a hybrid binder system containing 25% Portland cement, 50% calcined clay, and 25% limestone. Three alkali activators including sodium sulfate, sodium carbonate, and sodium metasilicate are evaluated at different alkali equivalent levels. Two reference systems were used for performance evaluation: a non-activated calcined clay composite cement and a blend containing 25 wt% Portland cement and 75 wt% limestone. The influence of activator mixing method (dry vs. pre-dissolved) is also examined.

The binder composition consisting of 25 wt% Portland cement, 50 wt % calcined clay, and 25 wt% limestone was selected to establish an ultra-low-clinker system in which hydration behavior is governed by the balance between calcium availability, reactive aluminosilicate content, and carbonate supply. The clinker fraction was intentionally limited to 25% to investigate hydration under conditions of restricted calcium availability. Compared with systems containing higher clinker contents, reduced portlandite availability increases the sensitivity of reaction pathways to pore solution chemistry and external alkali supply, allowing activator-specific effects to be more clearly distinguished.

A high calcined clay content (50%) was adopted to ensure a substantial supply of reactive alumina and silica, thereby promoting significant secondary reactions. Increasing the SCM fraction strengthens the chemical demand for calcium and amplifies the sensitivity of hydration pathways to changes in activator chemistry. The limestone content (25%) provides a defined carbonate background relative to the alumina supplied by the calcined clay. The 2:1 clay-to-limestone mass ratio follows proportions commonly adopted in LC^3 -type binders and has been shown to provide sufficient carbonate relative to reactive alumina to influence AFm phase development [26]. In the present work, this proportion was selected to ensure that carbonate availability does not become a limiting variable in hydrate evolution, allowing differences in phase assemblage and strength development to arise primarily from calcium availability and activator chemistry.

Because the extensive clinker dilution reduces the intrinsic alkali content of the binder to approximately 0.1 wt% Na_2O_{eq}, substantially below conventional Portland cement and typical LC^3 systems [27], external alkali addition becomes necessary to sustain pore solution alkalinity and promote early reactions. Previous LC^3 studies have explored moderate alkali adjustments around 0.8–1.2 wt% Na_2O_{eq} [14], but those systems retain higher clinker fractions and buffering capacity than the present formulation. Accordingly, an alkali level of 1.5 wt% Na_2O_{eq} was selected as a moderate alkalinity restoration level sufficient to enhance early hydration while remaining below typical alkali-activated binder dosages. A higher level of 3 wt% Na_2O_{eq} was included to explore the transition toward alkali-activation behavior. Alkali-activated systems commonly employ Na_2O contents beginning around 2–4 wt% and extending higher [6,28], so 3 wt% represents an approximate lower-bound activation regime that allows investigation of alkali effects without reaching strongly alkaline geopolymer conditions.

To investigate how activator chemistry influences hydration and strength development, three sodium-based activators were selected based on their distinct chemical roles and relevance to hybrid binder systems: sodium sulfate (Na_2SO_4), sodium carbonate (Na_2CO_3), and sodium metasilicate (Na_2SiO_3). These activators introduce different anionic species (SO_4^{2-}, CO_3^{2-}, and SiO_3^{2-}), enabling assessment of how alternative reaction pathways affect phase assemblage and microstructural evolution. Sodium sulfate represents sulfate-controlled activation and can accelerate hydration [9] while promoting ettringite formation and influencing AFt/AFm equilibria in alumina-rich systems [24]. Sodium carbonate represents carbonate-controlled activation; in calcined clay–limestone systems, carbonate ions participate in calcium–aluminate reactions leading to hemicarbonate and monocarbonate formation, which contribute to matrix densification and porosity refinement [29]. Sodium metasilicate represents silicate-controlled activation and supplies soluble silicate species that can directly influence C–(A)–S–H formation and early hydration kinetics [16], particularly in binders with limited clinker-derived silicate.

Together, the selected binder proportions, activator types, and alkali levels create a system in which calcium availability is intentionally limited and pore solution chemistry is externally controlled. Under these conditions, differences in hydration kinetics, phase assemblage, and strength development can be directly related to the type and amount of added activator. By evaluating the activators at identical Na_2O_{eq} levels, the influence of the accompanying anions (SO_4^{2-}, CO_3^{2-}, and SiO_3^{2-}) can be compared under consistent conditions, while recognizing that the optimal dosage for each activator may differ in practice.

A multi-technique approach including compressive strength testing, isothermal calorimetry, X-Ray diffraction (XRD), thermogravimetric analysis (TGA), mercury intrusion porosimetry (MIP), Brunauer–Emmett–Teller specific surface area analysis (BET), and dynamic vapor sorption (DVS) employed to establish a clear connection between mechanical performance and hydration behavior. By integrating these methods, the research aims to provide a deeper understanding of how different alkalis and mixing methods influence both the microstructural evolution and strength development of ultra-low clinker hybrid binders.

The goal of this study is to answer following key research questions:

- How does a low-clinker hybrid binder system (<25% clinker) perform in terms of early and long-term strength compared to reference systems, and what mechanisms govern this behavior?
- What is the impact of alkali activator mixing method (dry vs. predissolved) on mechanical performance?
- How do Na_2SO_4, Na_2CO_3, and Na_2SiO_3 affect the hydration kinetics of ultra-low clinker calcined clay-based binders?
- Do these activators differ in their impact on strength development? If so, what mechanisms, such as changes in porosity or phase assemblage, explain these differences?

2. Materials and methods

2.1. Materials

2.1.1. Raw materials

The binder system used in this study includes industrial Portland cement (CEM I 52.5 R), calcined clay, and limestone. The chemical compositions and mineralogical compositions of the raw materials were determined by X-ray fluorescence (XRF) and X-ray diffraction (XRD), respectively, and are summarized in Tables 1 and 2. Component densities used for binder volume calculations are summarized in Table S1.

2.1.2. Chemicals

Three alkali activators were selected to investigate their influence on hydration and mechanical performance including sodium sulfate decahydrate ($Na_2SO_4.10H_2O$), sodium carbonate anhydrous (Na_2CO_3), and sodium metasilicate pentahydrate ($Na_2SiO_3.5H_2O$). The sodium metasilicate used in this study was a laboratory-grade solution, distinct from commercial water glass, which typically contains higher silica content.

Table 1
Chemical composition of the raw material determined by XRF (wt%).

	CEM I 52.5 R	Calcined clay	Limestone
LOI 1050 °C	1.58	2.36	42.08
SiO_2	20.36	60.24	1.98
Al_2O_3	5.56	25.79	0.53
TiO_2	0.28	1.26	0.04
MnO	0.05	0.00	0.05
Fe_2O_3	2.39	8.87	0.30
CaO	62.17	0.98	54.10
MgO	1.66	0.24	0.61
K_2O	0.90	0.17	0.08
Na_2O	0.16	0.00	0.00
SO_3	3.90	0.05	0.11
P_2O_5	0.10	0.02	0.01
total XRF - 1050 °C	99.10	99.99	99.87

Table 2
Mineralogical compositions of the raw material (wt%).

	CEM I 52.5 R	Calcined clay	Limestone
C3S (M1)	14.6	-	-
C3S (M3)	39.7	-	-
C3S (total)	54.3	-	-
C2S (beta)	17.8	-	-
C2S (alpha)	1.9	-	-
C2S (total)	19.8	-	-
C3A (cub)	7.7	-	-
C3A (ortho)	3.5	-	-
C3A (total)	11.1	-	-
C4AF	5.3	-	-
Free lime	0.1	-	-
Portlandite	0.4	-	-
Periclase	0.7	-	-
Arcanite	1.3	-	-
Aphthitalite	0.4	-	-
Anhydrite	2.1	-	-
Hemihydrate	2.3		
Quartz	0.3	27.4	0.9
Calcite	1.9	1	95.9
Dolomite	-	-	2
Magnesite	-	-	0.3
Muscovite-2M1	-	-	0.9
Microcline max	-	2.3	-
Hematite	-	5.8	-
Anatase	-	0.7	-
Amorphous content	-	62.8	-

2.2. Experimental design

This study investigates hybrid cementitious systems based on a fixed binder ratio of 25% CEM I, 50% calcined clay, and 25% limestone, corresponding to a 1:2:1 ratio of CEM I: calcined clay: Limestone by mass. Two reference systems were included to isolate the effects of supplementary cementitious materials (SCMs) and alkali addition: A limestone-rich reference (REF-L75) containing 25% CEM I, and 75% limestone and a ternary SCM reference (REF-CC50) with 25% CEM I, 50% calcined clay, and 25% limestone without alkali activator. Three alkali activators, sodium carbonate (NC), sodium sulfate decahydrate (N$), and sodium metasilicate pentahydrate (NSi), were incorporated at alkali equivalent levels (Na_2O_{eq}) of 1.5%, and 3.0%, relative to the total binder mass. In case of sodium sulfate, three additional alkali levels of 0.5%, 1.0%, and 2.0% were also studied. Sodium carbonate and sodium sulfate were introduced using two methods: one approach was predissolving in water and the other was dry-mixing with the binder. For consistency in comparison, the activator percentages reported in Table S1 represent the solid content of each compound. For sodium

sulfate decahydrate and sodium metasilicate pentahydrate, the actual mass added was recalculated to achieve the target solid fraction, accounting for their crystalline water. This water was considered in the total mixing water, and the remaining water was adjusted so that all mixtures maintained a constant water-to-binder ratio of 0.50 by mass.

The experimental program was structured as follows:

- Mechanical performance was evaluated for all activator types, dosages, and mixing methods mentioned in Table S1
- Microstructural characterization (XRD, TGA, MIP, DVS) was focused on both reference systems and all three alkali activated systems with 1.5% Na_2O_{eq}, to reduce experimental effort while capturing representative trends.

The full testing matrix is presented in Table S1, and a schematic overview of the experimental matrix is shown in Fig. 1. Mix codes follow a structured format: the first letters indicate the activator type (e.g., N$ = sodium sulfate, NC = sodium carbonate, NSi = sodium metasilicate). The first number denotes the target Na_2O_{eq} coming from each activator, as wt% of binder. Since CEM I content is fixed and consistently provides ~0.1% Na_2O_{eq}, this does not affect comparability across mixes. The final letter specifies the incorporation method (P = pre-dissolved, D = dry-mixed). Additional suffixes describe storage conditions before casting: 24 h indicates dry-mixed blends stored < 24 h under standard lab conditions, whereas Lab denotes storage for less than one month.

2.3. Mortar and paste preparation

Mortar binders were prepared using a water-to-binder (w/b) ratio of 0.50 and a binder-to-sand ratio of 1:3 by mass. Mixing was conducted in accordance with EN 196–1 [30]. A rest interval was included during which manual mixing was performed to ensure homogeneity.

Alkali activators were incorporated either by pre-dissolving them in the mixing water or by dry blending with the binder prior to water addition. For sodium sulfate decahydrate, two dry mixing conditions were investigated: (i) casting within 24 h after mixing, and (ii) delayed casting after storing the dry blend for one month.

Paste samples were prepared at a water-to-binder ratio (w/b) of 0.50. Compressive strength testing showed no significant difference between pre-dissolving and dry-mix addition for sodium carbonate and sodium sulfate decahydrate when samples were cast within 24 h; therefore, the dry-mix addition approach was selected for both activators. For sodium metasilicate pentahydrate, only the pre-dissolved addition method was employed, as this was the sole addition route investigated for this activator. All pastes were mixed using an IKA T 50 Ultra-Turrax laboratory disperser equipped with a steel-rod stirrer. The mixing protocol consisted of 1 min of mechanical mixing at approximately 3000 rpm, followed by a 30 s rest period with manual stirring, and a final 1 min of mechanical mixing at a higher speed.

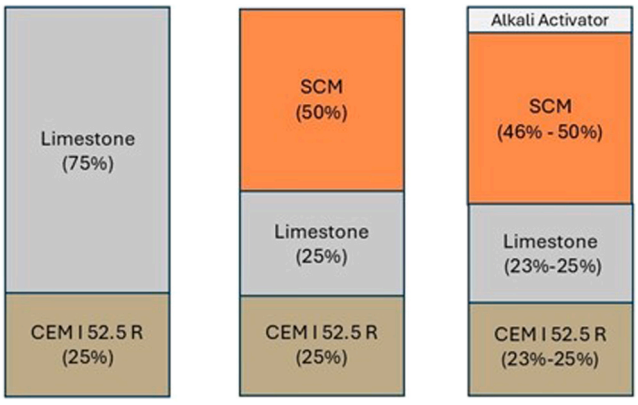

Fig. 1. Schematic overview of the experimental matrix.

Fresh pastes were cast into cylindrical plastic containers (35 mm diameter) and sealed with a lid and parafilm to minimize air exposure. Samples were stored at 20 °C until further processing. For analytical purposes, the central portion of each paste sample was used to avoid edge effects. Fresh disk specimens (without hydration stoppage) were used for dynamic vapor sorption (DVS) analysis. To investigate hydration products, additional samples were subjected to hydration stoppage. Hydration was stopped using an isopropanol-based solvent-exchange procedure with a subsequent petroleum ether rinse, adapted from published protocols [31,32]. The exact amounts used in this study include 10 g of material passed through 2 mm sieve and retained on 1 mm sieve, which was immersed in 150 mL of isopropanol for 10 min, followed by filtration and a 1-minute wash with petroleum ether. The same procedure was applied to the fraction passing the 1 mm sieve, using 15 g of material in 200 mL of isopropanol, followed by petroleum ether wash with equal volume. All solvent-treated samples were stored in vacuum desiccators at 20 °C for a period ranging from 4 days up to 1 week prior to measurement. After stoppage, the > 1 mm fraction was used for mercury intrusion porosimetry (MIP), while the < 1 mm fraction was ground to < 63 μm for XRD, XRF, TGA, and BET surface area analysis.

2.4. Experimental methods

2.4.1. Compressive strength testing

Mechanical performance was evaluated using prismatic mortar specimens measuring 40 × 40 × 160 mm, in accordance with EN 196–1 [30]. After mixing and molding, specimens were cured at 20 ± 1 °C and ≥ 90% RH until testing. Compressive strengths were determined on prism halves, and the average compressive strength was reported. Tests were performed at 2, 7, 28, and 90 days using a calibrated testing machine.

2.4.2. Isothermal calorimetry

Isothermal heat flow calorimetry was performed using a 3rd-generation TAM Air calorimeter (TA Instruments) equipped with eight independent measurement channels, maintained at 20 °C. For each test, 6.00 g of dry binder were weighed into a 20 mL glass ampoule and combined with 3.00 g of deionized water (w/b = 0.50). Ampoules were immediately sealed, handled only at the neck to avoid thermal disturbances, and homogenized for approximately 30 s on a shaker. Each sample channel was paired with its own sealed empty reference ampoule. Heat flow and cumulative heat release were recorded continuously for 7 d at a measurement interval of 57 s. Results are reported per gram of binder (cement, SCMs, and activator solids) without additional normalization. For comparison, calorimetry results expressed per gram of cement are included in the Supplementary Material.

2.4.3. Thermogravimetric analysis (TGA)

Thermogravimetric analyses were performed using a NETZSCH 209 F1 Libra system equipped with a QMS 403 D quadrupole mass spectrometer. Approximately 30 ± 2 mg of material was placed in open crucibles and heated under a nitrogen atmosphere. The temperature was increased from ambient conditions to 950 °C at a constant ramp of 20 °C/min.

Quantification of bound water and portlandite was based on mass loss observed between 50–550°C and 380–500°C respectively, applying Eq. (1) [33] and (2) [32]:

$$BW\ (wt.\%) = \frac{M_{50℃} - M_{550℃}}{M_{550}℃} * 100\% \quad (1)$$

$$CH\ (wt.\%) = \frac{CH_{TG}.M_{CH}/M_{H_2O}}{M_{600℃}} * 100\% \quad (2)$$

In this context, BW refers to the bound water content, and CH represents the portlandite fraction as wt% of the dry binder (M600°C). CH_{TG}

is the loss of water as a percentage of the initial sample mass attributed to calcium hydroxide decomposition. M_{CH}, and M_{H_2O} represent the molar masses of portlandite and water which are 74, and 18 g·mol^{-1}, respectively. The weight at 600°C (M600°C) was used as a reference point for quantifying portlandite contents. The tangent method was employed to determine CH_{TG} values. Total pore volume changes during hydration were also derived from TGA data using Eq. (3) [33]. Unreacted or free water, remaining from the original mixing process, was calculated and expressed relative to the initial paste volume. Changes in total volume due to autogenous (chemical) shrinkage were not included; since chemical shrinkage generates additional pore space, the calculated porosity therefore represents a lower-bound estimate of the true pore fraction.

$$P\,(Vol.\%) = \frac{V_{Pore}}{V_{Water} + V_{Binder}} * 100\% = \frac{V_{Water} - \frac{BW * m_{Binder}}{\rho_{BW} * 100\%}}{V_{Water} + \frac{m_{Binder}}{\rho_{Binder}}} * 100\% \quad (3)$$

Here, P is the pore volume %, V_{water} and M_{water} refer to the volume and mass of mixing water (with V_{water} assumed to equal M_{water} under a density of 1 g/cm^3), V_{Binder} and M_{Binder} are the volume and mass of whole binder, and BW is the bound water measured at a given time. The density of chemically bound water was taken as 1.3 g/cm^3, as commonly assumed in literature [34]. Binder volume was calculated from the true density of each raw powder component, using a rule of mixtures [35]:

$$\rho_{binder} = \frac{m_{binder}}{\sum_i \left(\frac{m_i}{\rho_i}\right)} \quad (4)$$

$$V_{Binder} = \frac{m_{Binder}}{\rho_{Binder}} \quad (5)$$

where m_i is the mass fraction of component i in the binder and ρ_i its true density. For hybrid systems, sodium carbonate and sodium sulfate were included in the binder mixture density, while sodium metasilicate was treated as a dissolved species and excluded from the binder volume; its carrier water was added to the mixing water. Component densities are summarized in Table S2 in the Supplementary Material section.

2.4.4. X-ray diffraction (XRD)

X ray diffraction (XRD) was used to characterize the crystalline phase assemblages in hydration-stopped and in-situ paste samples. Hydration-stopped samples were analyzed using a Bruker D8 Endeavor diffractometer equipped with an 8 mm stainless-steel front-loading sample holder, while in situ samples were measured using a Bruker D8 Advance diffractometer operated with a 15 mm front-loading holder.

Hydration-stopped samples were prepared by solvent exchange and subsequently stored in a vacuum desiccator. Before analysis, they were finely ground, sieved to < 63 μm, and homogenized. In-situ samples were prepared as sawn slices, mounted in the recessed holder with a support medium, and aligned so that the specimen surface was flush with the holder edge.

Measurements on the D8 Endeavor were performed in continuous scan mode from 4.0° to 72.0° 2θ, using a step size of 0.019° 2θ and an integration time of 0.6 s per step. A Cu Kα radiation source (λ = 1.5406 Å) was operated at 40 kV and 40 mA, and diffraction data were collected using a LYNXEYE position-sensitive detector. Samples were rotated at 15 rpm during acquisition to reduce preferred-orientation effects. Measurements on the D8 Advance were conducted in continuous coupled θ–2θ geometry over 4.0–72.0° 2θ, with a step size of 0.020°, using Cu Kα radiation (λ = 1.5406 Å) at 40 kV and 40 mA.

2.4.5. Mercury intrusion porosimetry (MIP)

Mercury intrusion porosimetry (MIP) was carried out using a Pascal 140/440 porosimeter system. Hydration was stopped with isopropanol and the material was gently crushed and sieved to obtain 1–2 mm fragments. To ensure complete removal of residual solvent before MIP measurement samples were placed in a desiccator at approximately 200–300 mbar for 7 days before measurement. Although crushing can generate artificial microcracks that slightly coarsen the measured pore structure [36] and sample preparation may also introduce microcracking through drying-related damage [37], these effects occurred uniformly across all mixtures and therefore did not bias the comparative analysis. Low-pressure (Pascal 140) and high-pressure (Pascal 440, up to 400 MPa) intrusion curves were recorded and corrected using the corresponding dilatometer blank file. The two pressure ranges were then combined, and the intrusion data were converted to pore diameter using the standard Washburn equation with a mercury contact angle of 140° and a surface tension of 0.48 N/m. Pore size distributions were obtained from the first derivative of the cumulative intrusion curve using the instrument's default smoothing routine. For very early-age samples exhibiting anomalously high low-pressure intrusion, only the high-pressure segment was used for interpretation.

MIP was used to characterize the pore structure through analysis of total intruded porosity and pore size distributions (PSDs). The total porosity obtained from MIP provides a measure of the fraction of the pore network accessible to mercury intrusion, while the PSDs describe the distribution of this porosity across different pore size ranges. The critical pore diameter (CPD) was used as a characteristic parameter of pore structure. CPD is defined as the pore diameter corresponding to the main peak in the differential intrusion curve above the gel-related pore range and represents the most frequent pore entry size controlling mercury intrusion. This parameter was extracted from the differential intrusion curves for each sample.

While CPD provides information on the dominant pore entry size, it does not describe how porosity is distributed within the accessible pore network. To compare differences in pore structure across binders, the fraction of pores accessible to mercury intrusion was evaluated using two pore-size windows, 20 nm–5 μm and 50 nm–5 μm. This analysis focuses on the coarser part of the pore network measured by MIP, while reducing the contribution from finer gel-scale porosity. The lower cutoff of 20 nm was selected as a conservative threshold to limit the influence of gel-related pores, while the 50 nm cutoff was chosen following the pore size distribution interpretation proposed by Muller and Scrivener [38], in which the valley between finer and coarser pore populations is used as a practical boundary. Pores larger than 5 μm were excluded from this analysis, as their contribution was negligible for all samples and such features are more likely associated with entrapped air or sample preparation effects rather than intrinsic hydration-related porosity.

For each pore-size window, the intruded pore volume was obtained from the cumulative mercury intrusion curve by subtracting the cumulative intrusion volume at the upper bound from that at the lower bound. The resulting volume was normalized by the total intruded pore volume measured by MIP and multiplied by the total MIP porosity to express the results as a percentage of material volume.

In addition, for the 50 nm–5 μm window, the pore volume was further subdivided relative to the critical pore diameter. The fractions of pores finer than the CPD and larger than the CPD were quantified to assess the distribution of the pore population with respect to the dominant pore entry size.

2.4.6. Dynamic vapor sorption (DVS)

Dynamic vapor sorption measurements were conducted using a DVS Adventure gravimetric sorption analyser (Surface Measurement Systems). Powdered paste samples (~30 mg) were loaded into stainless-steel pans. All experiments were performed at a controlled incubator temperature of 20 °C, with temperature stability confirmed by the measured incubator trace. Nitrogen was used as the carrier gas, and the total gas flow rate was maintained at 400 sccm (standard cubic centimeters per minute) during all runs. A data-logging interval of 60 s was used.

The humidity program began at 98% RH, followed by stepwise desorption to 5% RH, subsequent re-adsorption up to 60% RH, and a final desorption step at 5% RH.

Relative humidity steps were controlled using a mass-change rate equilibrium criterion: Each RH step was held until the mass-change rate fell below 0.00025% min^{-1} for at least 10 min. Total measurement time was approximately 10–12 days per run.

For the sodium sulfate decahydrate measurement, the same instrument was used, and temperature control, carrier gas, and data-logging conditions were identical to the cement samples. The sample was subjected to a stepwise RH from 98% to 0% and 0–98% back again, with each humidity step held until the mass change rate stabilized (minimum stage time 5 min, maximum 360 min, and a stability-duration setting of 10 min), and steady-state mass values determined from the final measurements at each setpoint.

2.4.7. BET N2 and BET Vapor

Specific surface area was measured by nitrogen adsorption at 77 K using a NOVA Touch NT4LX-1 (Quantachrome) analyser with TouchWin software. Samples (<63 μm) were outgassed under vacuum at 80 °C for 90 min after reaching temperature to remove adsorbed moisture. Adsorption–desorption isotherms were recorded automatically, and the multi-point BET surface area was calculated using the instrument software, assuming a nitrogen molecular cross-section of 0.162 nm^2 [39].

BET–H_2O specific surface area was determined from dynamic vapor sorption (DVS) data using the adsorption branch. The water uptake was defined relative to a reference dry mass (Eq. 6) following the common practice of normalizing sorbed water to a low-RH dry reference [40], In this study, the mass at 5% RH was used as a consistent reference state.

$$u = \frac{m - m_{5\%}}{m_{5\%}} \, g \Big/ g \tag{6}$$

where m is the equilibrium sample mass at a given relative humidity (RH), and $m_{5\%}$ is the equilibrium mass at 5% RH. The BET equation was applied in its linearized form [40,41]:

$$Y = \frac{x}{u(1-x)}, \quad x = \frac{RH}{100} \tag{7}$$

Linear regression of Y versus x was performed over the RH range of 20–40%, which consistently yielded high linearity. From the slope (s) and intercept (i) of the regression, the BET monolayer capacity u_m and BET constant C were calculated as [40,41]:

$$u_m = \frac{1}{(s+i)} \tag{8}$$

$$C = 1 + \frac{S}{i} \tag{9}$$

The specific surface area (SSA) was calculated as [41]:

$$SSA = u_m \times \frac{N_a \times \sigma}{M} \tag{10}$$

with N_a Avogadro's number, M the molar mass of water, and $\sigma = 0.114\ nm^2$ the molecular cross-sectional area of water molecules (converted to m^2 in calculations). This value of σ is consistent with recent applications of water-BET to cementitious systems [39,42]. Following the validity criteria for BET analysis proposed by Rouquerol et al. [41], only fits exhibiting high linearity within the selected pressure range were considered. In the present study, all selected fits showed $R^2 \geq 0.97$, indicating a high degree of linearity of the BET plots. As further noted by Rouquerol et al. [41], both the slope and intercept of the BET plot must be positive to ensure physically meaningful parameters. This requirement was fulfilled for all regressions in the present study, resulting in positive BET constants ($C > 0$). In addition, all calculated C values were greater than 2 [43], which further supports that the BET analysis was applied within a physically meaningful regime and that a well-defined monolayer region was obtained.

3. Results

3.1. Mechanical properties

3.1.1. Effect of alkali activator type and dosage on compressive strength

The compressive strength evolution of the reference system and alkali-activated systems (alkali pre-dissolved in water) is presented in Fig. 2. A comparison between REF-L75 and REF-CC50 reveals that the incorporation of 50% calcined clay has limited influence on early-age strength, with values increasing from 5.2 MPa to 7.2 MPa at 2 days. This reflects the slower kinetics of the pozzolanic reaction relative to the hydration of Portland cement, which typically dominates early-age strength development. However, by 28 days, the contribution of the pozzolanic reaction becomes more pronounced, with strength increasing to 25.8 MPa.

The effect of alkali activation varies significantly depending on the type and dosage of activator. At a low dosage (1.5% Na_2O_{eq}), Na_2SiO_3 enhances early strength to 10.9 MPa, but this improvement is accompanied by a substantial reduction in compressive strength at 28 days (≈-40%). Increasing the activator dosage to 3% Na_2O_{eq} for Na_2SiO_3 results in strength reduction across all studied ages. The Na_2CO_3-activated system could not be demolded after 24 h due to insufficient strength and required an extended curing period before demolding at 3 days. Both dosages of Na_2CO_3 resulted in strength reduction at all studied ages in comparison to REF-CC50.

In contrast, Na_2SO_4 exhibits a more favorable performance. At 2 days, compressive strength increased from 7.2 MPa (REF-CC50) to 18.8 MPa (+160% improvement). Although a slight reduction was observed at 28 days (from 25.8 MPa to 22.8 MPa), this decrease is the smallest among all activators tested.

3.1.2. Effect of pre-dissolving vs. dry mixing on compressive strength

Fig. 3 shows the influence of the activator incorporation method, pre-dissolution in water versus dry mixing with the binder, for Na_2CO_3 and Na_2SO_4 on compressive strength. The compressive strength results revealed negligible differences between the two methods in the case of Na_2CO_3. In contrast, for Na_2SO_4, dry mixing led to a significant reduction in strength compared to pre-dissolution. This behavior is attributed to the use of sodium sulfate decahydrate ($Na_2SO_4{\cdot}10H_2O$), which may partially release its crystalline water when in contact with the hydrophilic surfaces of cement particles during dry storage, promoting premature hydration and reducing the effective mixing water available during casting.

To test this hypothesis, dynamic vapor sorption (DVS) analysis was conducted on $Na_2SO_4{\cdot}10H_2O$. The results, shown in Fig. 4, demonstrated a significant mass loss when relative humidity dropped below 70%, indicating that $Na_2SO_4{\cdot}10H_2O$ begins to release crystalline water under typical laboratory conditions (RH < 70%). Although DVS operates under dynamic conditions that differ from static storage, the strength results and visual observations during mixing support this interpretation. Specifically, dry-mixed systems exhibited noticeably lower workability. This suggests that a portion of the crystalline water had already evaporated prior to mixing, resulting in an effective water deficit during mortar preparation. While workability was not quantitatively measured in this study, the reduction was clearly observed during mixing.

To mitigate this issue, a revised protocol was implemented in which $Na_2SO_4{\cdot}10H_2O$ was dry-mixed with the binder, sealed, and stored for less than 24 h before casting. In parallel, pre-dissolved systems were prepared at varying alkali-equivalent levels. Additional mixes with alkali equivalents of 0.5%, 1%, and 2% were included in this validation study to confirm that the observed trends were consistent across a broader dosage range. As shown in Fig. 5, when the activator was dry-mixed and cast shortly after preparation, the resulting strengths were very similar

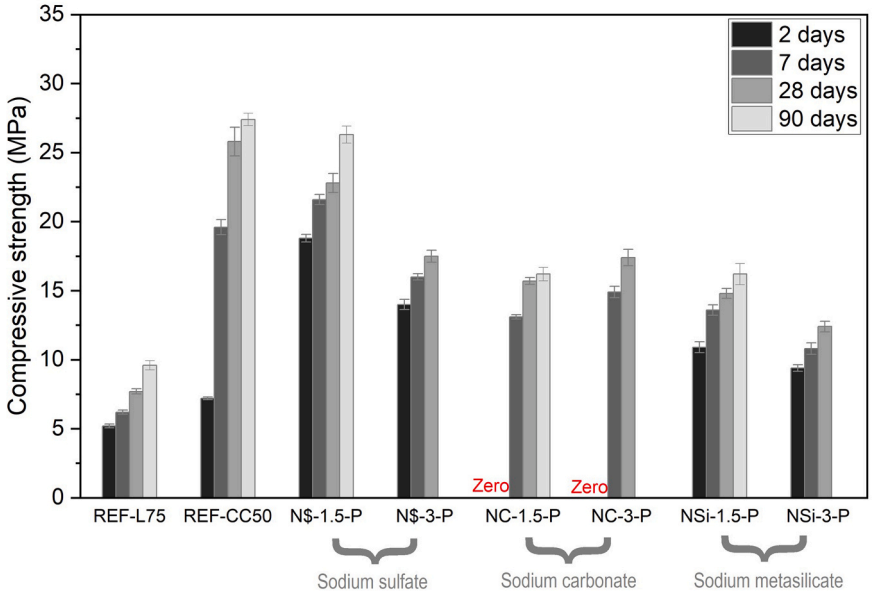

Fig. 2. Compressive strength development of mortar samples activated with different alkali types and dosages. All activators were pre dissolved in the mixing water. Strength testing at 90 days was conducted only for mixtures with the lower activator dosages.

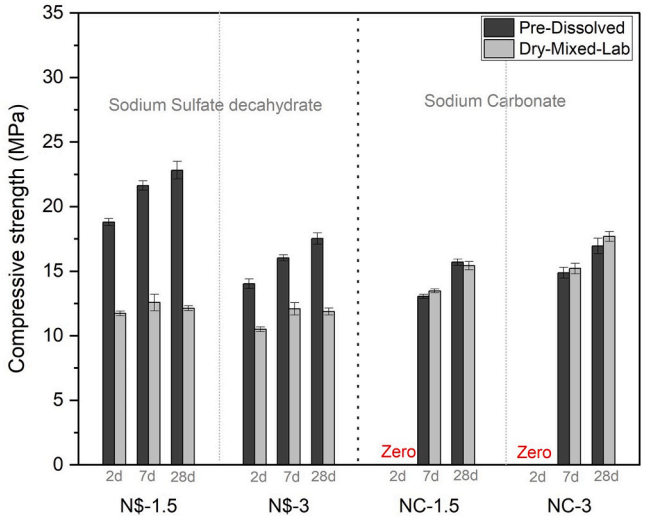

Fig. 3. Effect of activator incorporation method including pre dissolution versus dry mixing on the compressive strength of mortar samples.

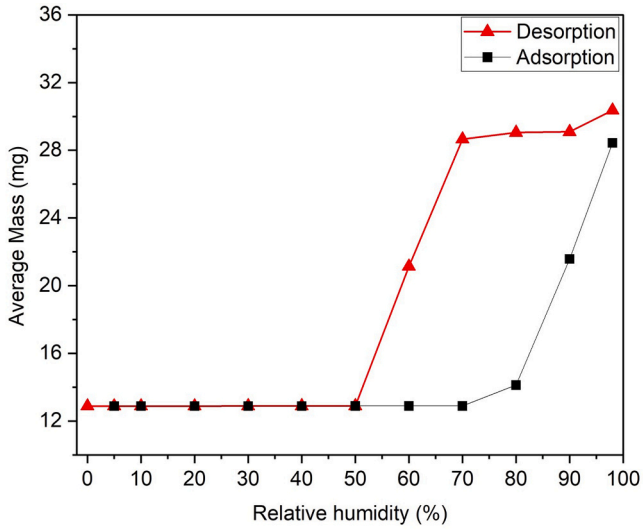

Fig. 4. Mass change of sodium sulfate decahydrate ($Na_2SO_4{\cdot}10H_2O$) during desorption–adsorption cycles under varying relative humidity.

to those obtained under pre-dissolution conditions.

3.2. Reaction kinetics from isothermal calorimetry

3.2.1. Influence of alkali type, dosage, and mixing method

For the reference REF-CC50 mix, isothermal calorimetry (Fig. 6a) revealed a delayed and suppressed alite (C_3S) peak, followed by a broad aluminate (C_3A) peak. The addition of Na_2SiO_3 significantly altered this hydration pattern (Fig. 6a). At a dosage of 1.5% Na_2O_{eq}, the first calorimetric peak shifted to within the first hour and increased in intensity from ~1.4 mW/g to ~2.8 mW/g, indicating accelerated early hydration. The second peak, associated with aluminate reactions, also intensified. At a dosage of 3.0% Na_2O_{eq}, the silicate peak was delayed (in comparison to the lower dosage) to ~2 h but intensified to ~5.8 mW/g. Despite these kinetic differences, cumulative heat measurements after 7 days were similar across both dosages (Fig. 6b).

Na_2CO_3-activated systems with 1.5% and 3.0% Na_2O_{eq} exhibited prolonged induction periods, with no distinctive calorimetric peak for the first two days (Fig. 6c). The timing of the first calorimetric peak was influenced by both the Na_2CO_3 dosage and the method of its addition (pre-dissolved or dry-mixed). The method of Na_2CO_3 addition caused additional shifts in peak timing; however, the direction of this effect was not consistent across dosages. At lower Na_2CO_3 contents, dry mixing resulted in a slightly earlier peak, whereas at higher contents it led to a slightly later peak compared with pre-dissolving (Fig. 6c). In all cases, these differences were limited to a few hours and were small relative to the overall induction period of > 50 h. This indicates that while Na_2CO_3 dosage has a clear influence on reaction delay, the addition method mainly affects early-age processes and does not bring a dominant or systematic control over the overall reaction kinetics. Cumulative heat measurements of both dosages after 7 days were less than the REF-CC50 (Fig. 6d).

The addition of Na_2SO_4 at 1.5% and 3.0% Na_2O_{eq} (pre-dissolving) resulted in a more intense first calorimetric peak (~7 mW/g) occurring

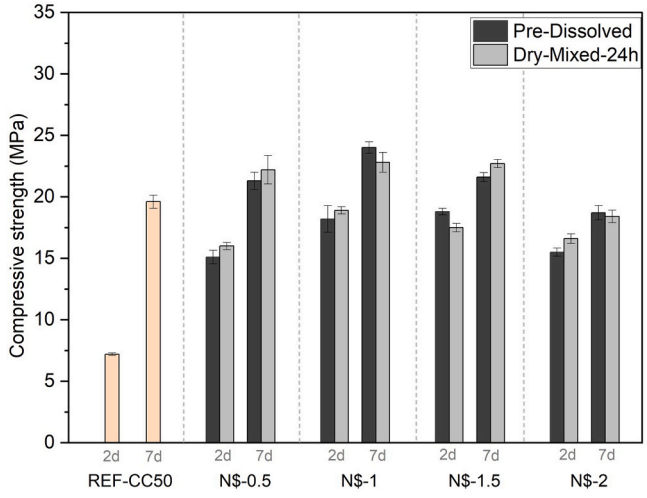

Fig. 5. Comparison of compressive strength between mortars prepared by dry-mixing (cast within 24 h of blending) and those prepared with pre-dissolved sodium sulfate decahydrate.

at approximately 6.5 h, without a noticeable earlier onset compared with the REF-CC50 system (Fig. 6e). When Na_2SO_4 was pre-dissolved, both 1.5% and 3.0% Na_2O_{eq} dosages produced cumulative heat values after 7 days comparable to those of the REF-CC50 system. The calorimetric response of the Na_2SO_4 system was also highly sensitive to the mixing and storage protocol. At 1.5% Na_2O_{eq}, when the dry-mixed binder was stored for more than 24 h prior to casting, the main hydration peak was significantly delayed and suppressed (Fig. 6e). At the higher Na_2O_{eq} dosage of 3.0% Na_2O_{eq}, dry mixing followed by storage for more than 24 h resulted in a much stronger inhibitory effect. The calorimetric signal was drastically suppressed, showing a broad, low-intensity peak (<1 mW/g) between approximately 1 and 6 h (Fig. 6e). The cumulative heat release in this case was less than 40 J/g, the lowest among all tested systems (Fig. 6f). The 1.5% Na_2O_{eq} dry-mixed system also exhibited low cumulative heat release, only slightly higher than that of the 3.0% system, confirming that extended dry storage significantly suppresses hydration. In both systems containing 1.5% and 3% Na_2O_{eq}, when the dry-mixed $Na_2SO_4{\cdot}10H_2O$ binder was cast within 24 h, the overall shape of the calorimetric curve was comparable to that of their corresponding pre-dissolved systems; however, the onset and maximum of the silicate peak were delayed by a few hours and the peak intensity was lower. This behavior is likely attributed to the dry addition of sodium sulfate, which requires dissolution of sodium oxide and sulfate after water addition, resulting in a slower availability of alkalinity and sulfate ions compared to the pre-dissolved condition.

Fig. 6g presents the heat flow during the first 30 min after water addition. The REF-CC50 paste shows a pronounced initial exothermic peak. A similar early peak (about 40 mW/g) is observed when Na_2SO_4 is introduced as a pre-dissolved solution. In contrast, when $Na_2SO_4{\cdot}10H_2O$ is introduced as a dry solid, the initial signal is strongly reduced. For the freshly prepared dry-mixed binders (cast within 24 h), the early signal decreases to about 6 mW/g at 1.5% Na_2O_{eq} and becomes net endothermic at 3.0% Na_2O_{eq} (minimum around −10 mW/g). After prolonged dry storage, the initial signal becomes very small, with a small positive response at 1.5% Na_2Oeq (≈10 mW/g) and close to zero at 3.0% Na_2O_{eq}.

3.3. Microstructural characterization

3.3.1. Bound water and portlandite quantification by TGA

Fig. 7 presents the bound water (BW) contents measured at 2, 7, 28, and 90 days for all investigated systems. In this study, BW was quantified from TGA using the mass loss between 50–550 °C, as described in 2.4.3. The full DTG curves for all binders are provided in Fig. S1. At all ages, the REF-L75 system exhibited the lowest BW content while the REF-CC50 system demonstrated significantly higher BW values. Specifically, REF-L75 increased from approximately 6.1 wt% at 2 days to 8 wt% at 90 days, whereas REF-CC50 ranged from 9.6 wt% to 12.4 wt% over the same period, confirming the higher overall degree of reaction in the calcined clay reference system. Among the alkali-activated systems, the Na_2SO_4-activated binder (N$-1.5-D-24 h) consistently exhibited the highest BW, particularly at early age (11.8 wt% at 2 days). The Na_2SiO_3-activated system (NSi-1.5-P) showed lower BW at 2 days (7.9 wt%) compared to REF-CC50 (9.6 wt%), despite exhibiting a 3–4 MPa higher compressive strength (Fig. 7). Across 2–90 days, NSi-1.5-P exhibited only minor variation in BW, ranging from 7.94 wt% at 2 days to 8.25 wt % at 90 days. Similarly, the Na_2CO_3-activated system showed a gradual increase in BW from 8.19 wt% at 7 days to 9.20 wt% at 90 days, indicating limited additional bound water formation after early hydration.

Portlandite evolution across the systems reflects distinct hydration and reaction mechanisms. In REF-L75, portlandite steadily increased over time (Fig. 8), indicating ongoing clinker hydration without secondary consumption. In REF-CC50, portlandite was depleted by 7 days, consistent with rapid pozzolanic reaction between $Ca(OH)_2$ and reactive aluminosilicates from calcined clay. In alkali-activated systems, portlandite was absent at all ages.

3.3.2. Phase development by XRD

XRD analysis (Fig. 10) reveals the evolution of crystalline phases, providing evidence of how activator chemistry governs hydration pathways and phase assemblage development. For the REF-L75 system (CEM I + limestone), monocarbonate was identified across all ages (Fig. 10a). In the REF-CC50 system (calcined clay + limestone + CEM I), both hemicarbonate and monocarbonate were detected at early ages (Fig. 10b). In the Na_2SO_4-activated system (N$-1.5-D-24 h), strong ettringite reflections were observed at 2 days and persisted at later ages (Fig. 10c). The Na_2SiO_3-activated paste (NSi-1.5-P) exhibited a distinct reflection at $2\theta \approx 8.8°$ (Fig. 10d), which matches the diffraction pattern of a Na-substituted AFm (U-phase). In the Na_2CO_3-activated system, neither ettringite nor AFm-carbonates were detected in the hydration-stopped specimens by XRD (Fig. 9e). Additionally, no evidence of strätlingite (C_2ASH_8) was detected in the XRD patterns of any system.

3.3.3. Pore structure characterization

Fig. 10 compares the total porosity obtained from TGA with the total intruded porosity measured by MIP. While individual curing ages are not distinguished in the scatter plot, the complete age-resolved porosity data for both techniques are provided in Table S3. In all systems, the TGA-derived porosities are higher than the corresponding MIP values. Despite the difference in absolute magnitude, both methods follow the same overall pattern: the reference systems (REF-L75 and REF-CC50) show a reduction in porosity with increasing curing time, while the alkali-activated systems show porosity values that remain largely unchanged between 2 and 90 days.

CPD was defined as the position of the main peak in the differential intrusion curve above the gel-related intrusion (~10 nm) [38,44]. The corresponding pore size distributions are presented in Fig. S2. The two reference binders exhibited a clear refinement of CPD with curing age, as shown in Fig. 11 (REF-L75: ~974 nm at 2 d decreasing to ~396 nm at 90 d; REF-CC50: ~471 nm decreasing to ~318 nm), consistent with the observed reduction in total porosity. In contrast, the alkali-activated systems, including Na_2SiO_3, Na_2SO_4 and Na_2CO_3-activated binders, showed only limited changes in CPD with hydration time (Fig. 11).

To compare differences in pore structure across binders, the fraction of pores accessible to mercury intrusion was evaluated using two pore-size windows, 20 nm–5 μm and 50 nm–5 μm (Fig. 12). Pore size distributions curves as presented in Fig. S2 show that the 50 nm cutoff effectively excludes the finer pore population and captures the coarser peak only. However, some binders displayed a single dominant peak rather than a clearly bimodal distribution. To enable consistent

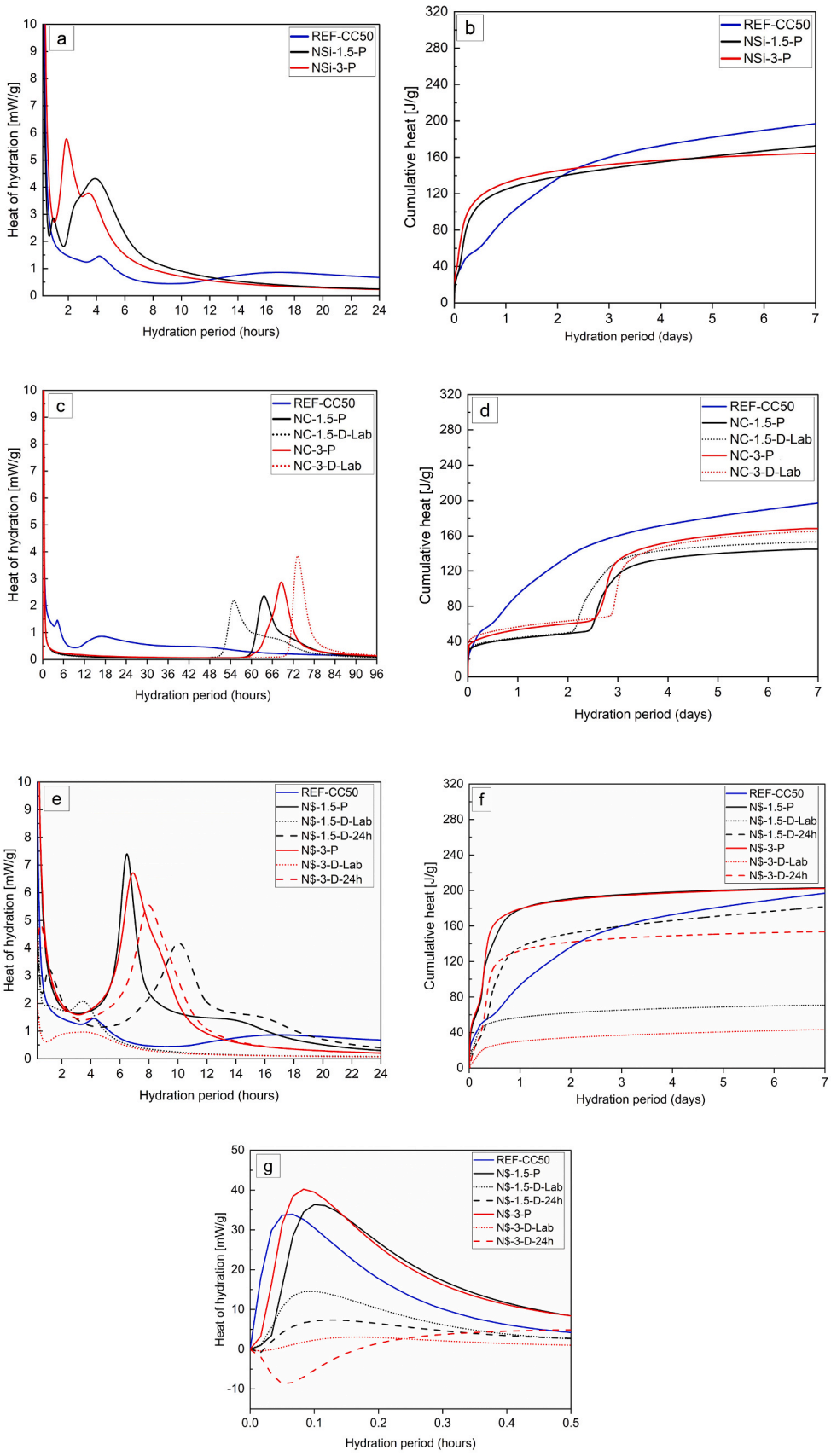

Fig. 6. Isothermal calorimetry results per gram of anhydrous binder, highlighting the influence of alkali activator type and mixing method. (a, b) correspond to sodium metasilicate, (c, d) to sodium carbonate, and (e, f, g) to sodium sulfate. Note: the time axis in panel (c) is extended to 96 h to display all heat flow peaks. (Isothermal calorimetry results per gram of cement is presented in Fig. S3).

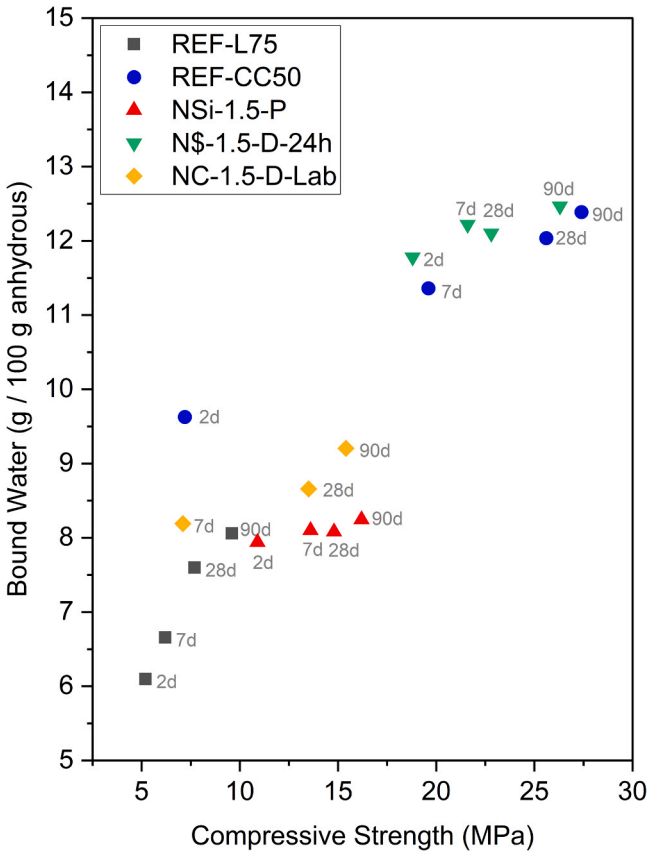

Fig. 7. Relationship between bound water content (determined by TGA) and compressive strength for the references and hybrid binders.

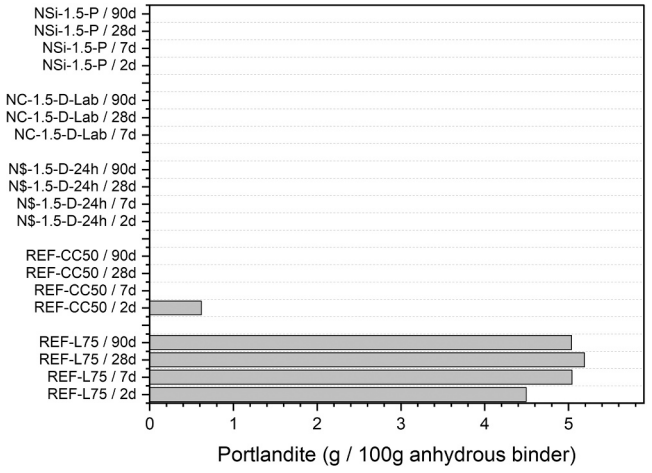

Fig. 8. Portlandite content quantified from TGA measurements at different curing ages.

comparison across all systems, a fixed lower bound of 50 nm was therefore applied, rather than adjusting the cutoff individually for each pore size distribution.

As shown in Fig. 12, at the 20 nm cutoff, both reference binders showed gradual coarse porosity reduction from 2d to 90d (REF-L75: ~41% → ~37%; REF-CC50: ~35% → ~29%), consistent with CPD refinement (Fig. 11). Activated systems remained largely unchanged, while Na_2CO_3 exhibited a slight increase (33% → 35%). At the 50 nm cutoff, the reference binders again refined systematically (REF-L75: ~38% → ~32%; REF-CC50: ~29% → ~24%), whereas activated systems followed similar patterns to the 20 nm window. The consistency of trends across both pore-size windows indicates that the limited pore refinement in the activated systems is not sensitive to the exact choice of lower cutoff.

To examine pore network organization beyond absolute porosity values, the predefined pore-size window of 50 nm–5 μm was subdivided into fractions finer and coarser than the critical pore diameter (CPD) (Fig. 13). This analysis provides information that is not captured by total MIP-accessible porosity alone, as it reveals whether changes in pore structure involve a redistribution toward finer or coarser pore entry sizes within the same pore-size domain. For all binders, pores finer than the CPD dominated at all ages. The fraction of pores finer than the CPD remained above 50% for all systems throughout the investigated curing period. Both references had the highest fraction of pores finer than the CPD. Among the alkali-activated systems Na_2SO_4 had the highest fine fraction while Na_2SiO_3 and Na_2CO_3 had significantly lower fraction of fine porosity. The Na_2SO_4-activated system maintained fine pore fractions between 64% and 68% over 2–90 days, consistently exceeding those of the Na_2SiO_3 and Na_2CO_3 systems. In contrast, Na_2SiO_3 showed a progressive reduction in fine fraction from 62.0% at 2 days to 50.9% at 90 days, approaching an approximately equal distribution of finer and coarser pores. Similarly, Na_2CO_3 exhibited relatively stable but lower fine fractions of approximately 54–56% between 7 and 90 days.

For both reference binders, a gradual increase in H_2O-BET was observed with curing age (Fig. 14). Specifically, REF-L75 increased from 30.4 m^2/g at 2 days to 43.8 m^2/g at 90 days (≈44% increase), while REF-CC50 increased from 46.5 m^2/g to 65.4 m^2/g over the same period (≈41% increase), indicating progressive development of hydrophilic surface area during hydration. In contrast, N_2 BET values for the reference systems remained relatively low and showed limited temporal evolution. For REF-L75, N_2-BET increased modestly from 12.3 m^2/g at 2 days to 16.8 m^2/g at 90 days, while REF-CC50 increased from 23.0 m^2/g to 29.2 m^2/g, indicating comparatively smaller changes in nitrogen-accessible surface area relative to H_2O-BET. This behavior is consistent with ongoing gel formation primarily affecting water accessible surfaces rather than nitrogen accessible ones. All three activated systems exhibited little to no change with curing age in either N_2-BET or H_2O-BET, indicating that surface accessibility is largely established at early ages. For example, NSi-1.5-P showed H_2O-BET values between 58.9 and 65.2 m^2/g and N_2-BET values between 13.7 and 15.5 m^2/g across 2–90 days. Similarly, N$-1.5-D-24h exhibited H_2O-BET values ranging from 63.9 to 68.4 m^2/g and N_2-BET values between 25.7 and 28.2 m^2/g. Similarly NC-1.5-D-Lab remained comparatively stable, with H_2O-BET between 52.7 and 55.8 m^2/g and N_2-BET between 20.0 and 21.4 m^2/g after 7 days. Among them, the Na_2SiO_3 and Na_2SO_4 activated binders showed the highest H_2O-BET values overall, reflecting the presence of extensive hydrophilic surface domains. In particular, N$-1.5-D-24h exhibited the highest combined surface accessibility, with H_2O-BET reaching 68.4 m^2/g at 90 days and consistently higher N_2-BET values (~26–28 m^2/g) compared to the other systems.

4. Discussion

4.1. Mechanistic interpretation of early hydration kinetics under different activators

To interpret the calorimetric responses observed for the different activators, the discussion below considers how early interactions among aluminates, silicates, and alkalis can influence dissolution and precipitation processes. While the individual mechanisms are not directly resolved in the present study, established findings from the literature, together with the experimental trends observed here, provide a consistent framework for interpreting the calorimetric behavior shown in Fig. 6.

Pore solution alkalinity is a key parameter influencing hydration kinetics and calorimetric behavior. In LC^3-50 systems (50% clinker, 30%

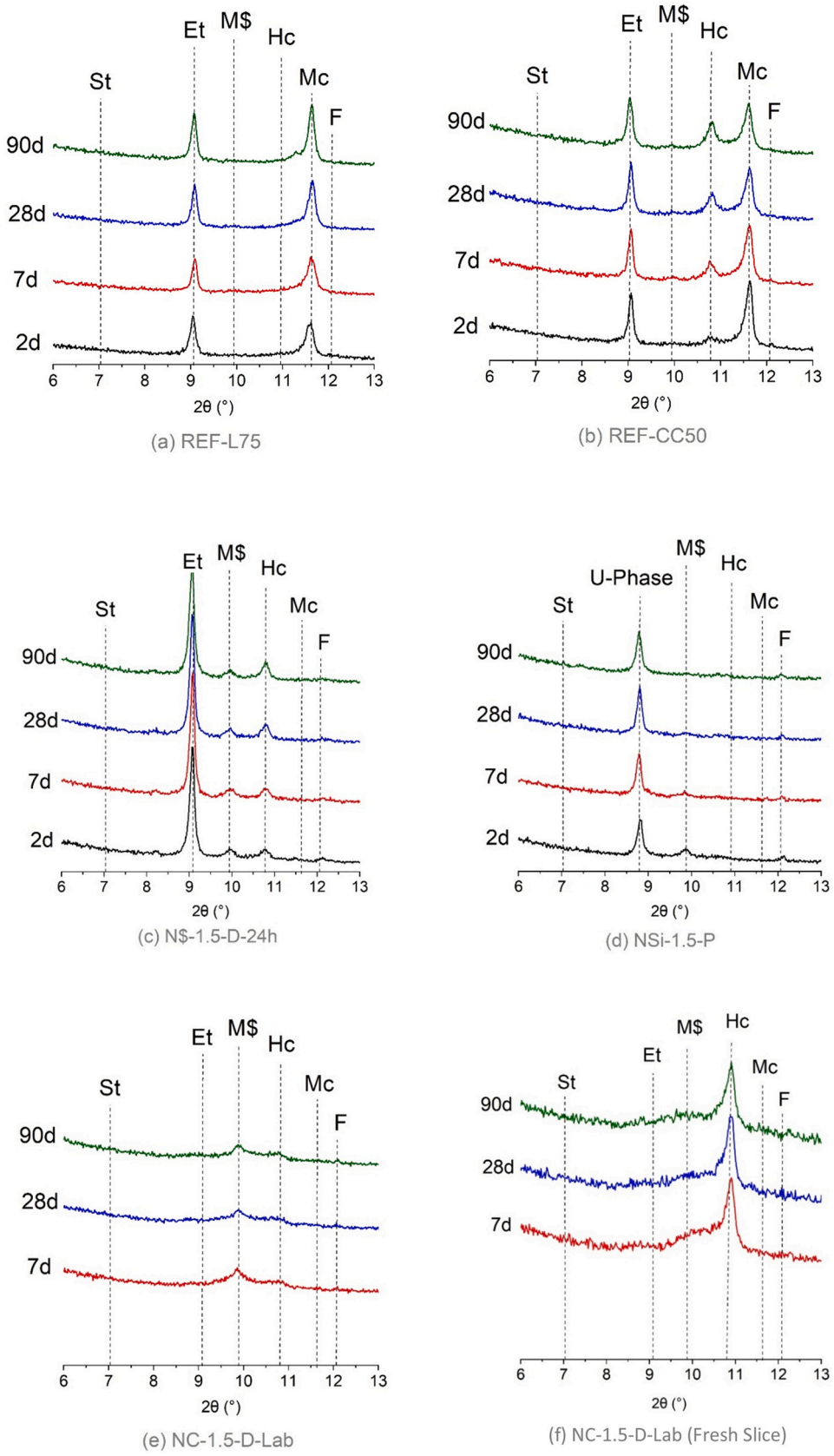

Fig. 9. XRD patterns of pastes after 2, 7, 28, and 90 days of hydration. (a)–(e) correspond to hydration stopped pastes; (f) presents the XRD pattern obtained from a fresh, unstopped slice.

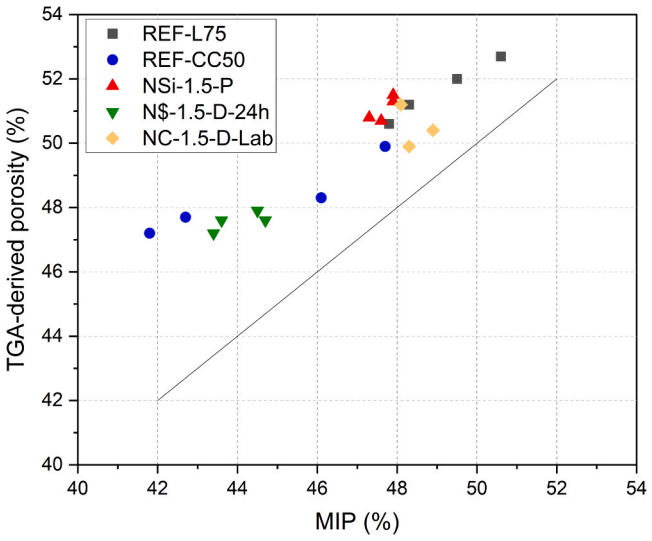

Fig. 10. Comparison of porosity values obtained from TGA (water mass balance approach) and MIP (data summarized in Table S3).

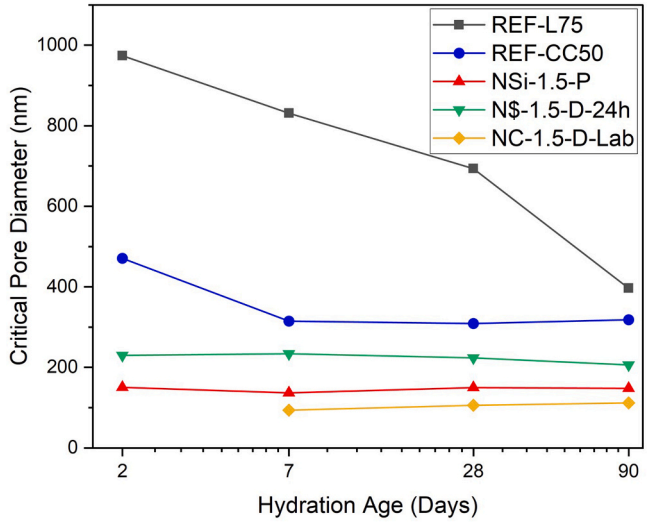

Fig. 11. Critical pore diameter determined from MIP at curing ages of 2, 7, 28, and 90 days.

calcined clay, 15% limestone), direct pore solution extraction measurements report pH values between 13.2 and 13.8, depending on calcined kaolinite content [27]. A slight decrease in pH with increasing calcined kaolinite content has been reported and attributed to alkali incorporation into hydration products formed during the metakaolin reaction, along with reduced calcium concentration due to portlandite consumption [45].

In our reference system (REF-CC50) the substantially lower clinker content, low alkali equivalent (~0.1% Na_2O_{eq}), and higher calcined clay fraction suggest a reduced intrinsic pore solution alkalinity compared to LC^3-50. Based on compositional comparison with the literature, a pore solution pH in the range of approximately ≈ 12–12.5 is expected in this system. This value is estimated from differences in clinker content and was not directly measured in this study.

For the activated systems, pore solution alkalinity depends on the activator. pH values for sodium silicate activation in LC^3 system (Ms ≈ 1) have been reported to be between 12.95 and 13.40, depending on Na_2O content [16] indicating strongly alkaline conditions. For comparison, the pH of the activators in aqueous solution has been reported to be approximately 12.6 for sodium carbonate and about 8 for sodium sulfate, compared to about 13.4 for sodium silicate, demonstrating the lower intrinsic alkalinity of sodium sulfate and carbonate [46]. Accordingly, He et al., [47] classified sodium sulfate and sodium carbonate as weakly alkaline relative to sodium silicate. Furthermore, Bernal et al. [48] showed that partial replacement of sodium carbonate with sodium silicate increases system alkalinity. Together, these studies confirm that carbonate- and sulfate-based activators operate in a lower alkalinity regime than silicate systems. Therefore, while the sodium silicate–activated system in the present study is expected to reach pH values above 13, the sodium sulfate– and sodium carbonate–activated systems are likely to exhibit pore solution pH values slightly higher than REF-CC50 but lower than those of the sodium silicate–activated system.

It should be noted that, in systems activated with mildly alkaline activators such as sodium sulfate and sodium carbonate, the pore solution pH is not governed solely by the initial alkalinity of the activating solution but rather evolves throughout hydration. Previous studies have shown that reactions between the activator and portlandite can initially contribute to an in situ increase in pH [20,21,49]. At later stages, however, the pore solution pH may decrease as pozzolanic reactions progress, due to portlandite consumption and the incorporation of alkali ions into C–A–S–H-type phases [22,25,49]. This in-situ development of alkalinity is one of the key advantages of mild activators, as it allows sufficiently alkaline conditions to be established within the system while avoiding the handling and safety concerns associated with highly caustic activating solutions.

Given that the pore solution pH in the REF-CC50 system is expected

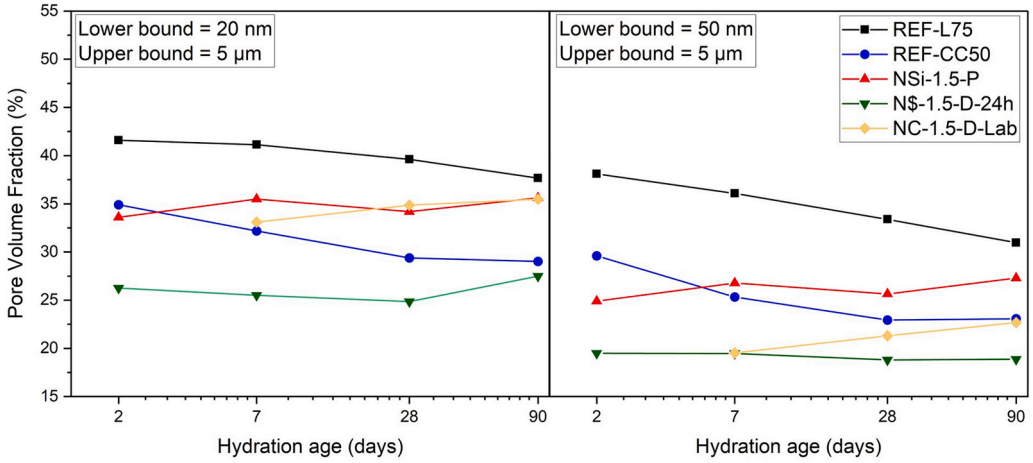

Fig. 12. Coarse porosity quantified from MIP data using two predefined pore size windows (for PSD curves see Fig. S2).

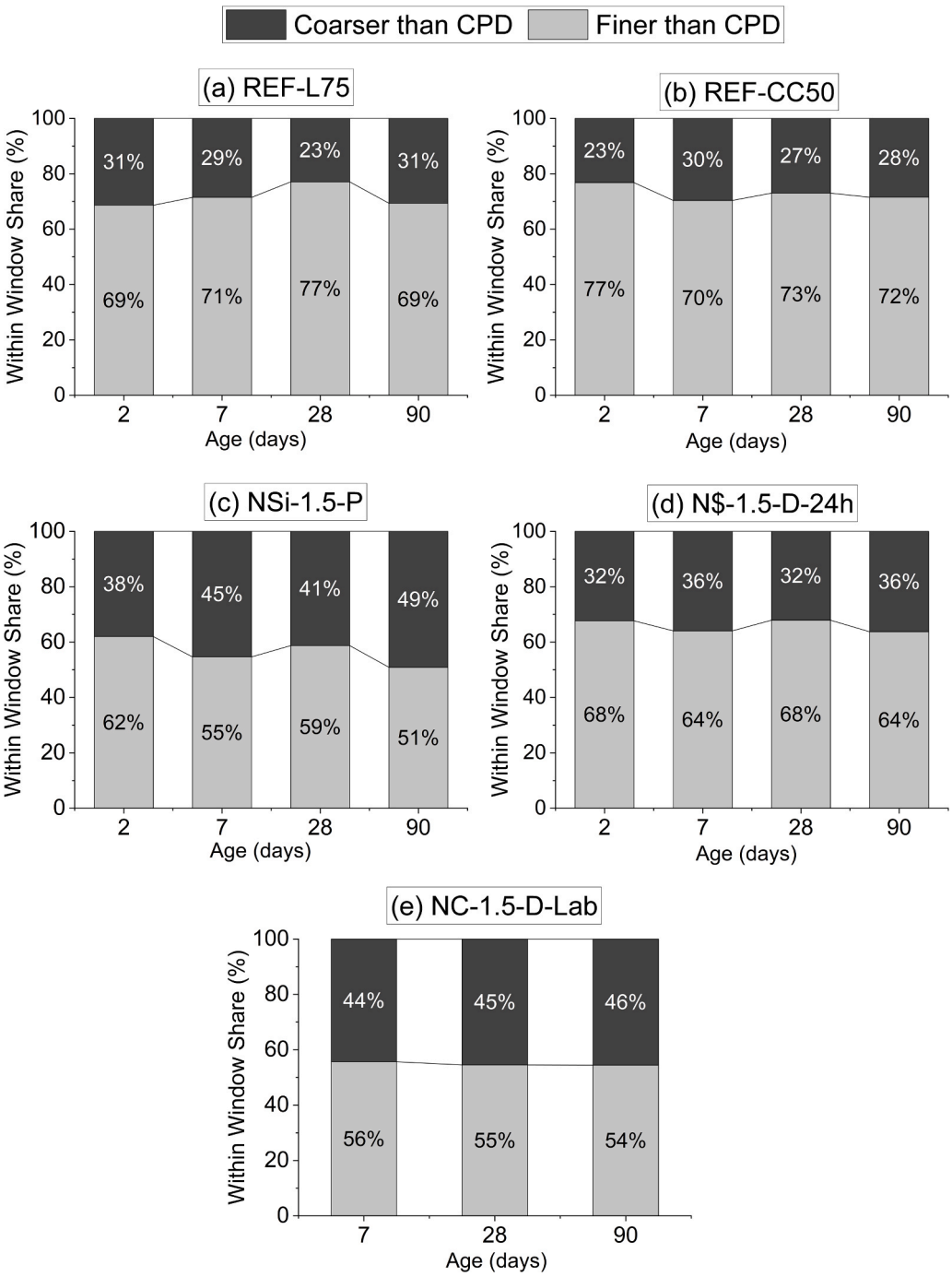

Fig. 13. Distribution of pores finer and coarser than the critical pore diameter within the MIP accessible window from 50 nm to 5 μm.

to lie in the mildly alkaline range (~12–12.5), interactions between dissolved aluminates and silicate surfaces are likely to be particularly significant during the early stages of hydration. Under such conditions, aluminate species can adsorb onto calcium silicate surfaces, potentially limiting C_3S dissolution. Consistent with this interpretation, the calorimetric response of REF-CC50 (Fig. 6a) shows a suppressed alite (C_3S) peak followed by a broad aluminate (C_3A) peak. This behavior is consistent with surface passivation of C_3S by aluminates, which hinders further dissolution and suppresses the development of a distinct silicate peak [50]. Pustovgar et al. [51] demonstrated that this adsorption occurs primarily through strong ionic interactions between aluminate and calcium ions. However, such passivating effect is pH-sensitive and can be mitigated in presence of higher pH. As hydration progresses or when alkali activators raise the pH, the abundance of OH^- and Na^+ ions compete with aluminates for surface sites, weakening their binding strength. Bagheri et al. [52] showed that silica dissolution increases slightly as pH rises from ~12.4–13.0, but the difference is within experimental error for amorphous silica. Aluminium significantly inhibits dissolution across this range, with the strongest effect at lower pH: at pH ≈ 12.4, 3 mM Al reduced the dissolution rate of amorphous silica by ~18 ×, while at pH ≈ 13 the reduction was ~4 ×. This trend is attributed to the decreasing sorption of Al on silica surfaces as pH increases, because Al species shift toward $Al(OH)_4^-$ at higher pH, which interacts less with silica. Zajac et al. [53] similarly propose that the inhibitory effect of aluminates on calcium silicate surfaces is strongest under mildly alkaline conditions and diminishes at higher pH,

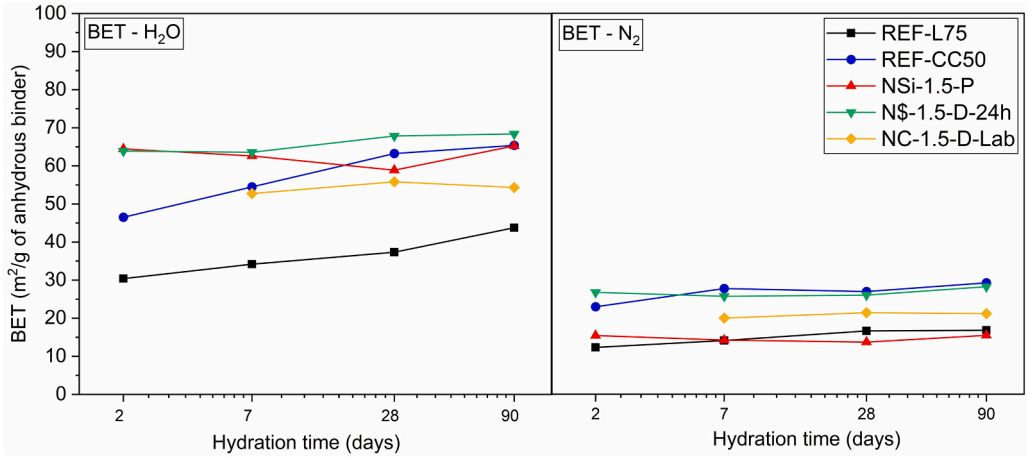

Fig. 14. Evolution of water-accessible surface area (H_2O-BET, calculated from DVS data) and nitrogen-accessible surface area (N_2-BET) at 2, 7, 28, and 90 days.

alleviating their retarding influence.

Upon addition of Na_2SiO_3, a small pre-induction period peak is observed which is likely attributed to the early precipitation of reaction products prior to the main acceleration peak. This heat release could be associated with the rapid release of ions into the pore solution and early Ca-related interactions or other solution-driven reactions occurring at very early ages. In studies on alkali activated fly ash/slag systems, similar pre-induction peaks have been reported and attributed to wetting and dissolution of the raw materials, as well as to the coagulation of dissolved silicate and aluminate species and their interactions with calcium and sodium [54].

The second peak by the addition of Na_2SiO_3 (Fig. 6a) is therefore attributed to the overlapping of C_3S and C_3A reactions. The intensified peak align with Dai et al. [16], who observed more pronounced C_3S and C_3A peaks in LC^3 systems upon Na_2SiO_3 addition at optimized level. The enhanced reactivity is attributed to the elevated pore solution pH, which promotes C_3S dissolution, and the availability of reactive silicate species that facilitate early nucleation of C–S–H. The delayed silicate peak in higher dosage of Na_2SiO_3 compared to the lower dosage could be related to the reduced ion mobility at higher dosage. Similar cumulative heat measurement after 7 days in both dosages of Na_2SiO_3 (Fig. 6b) suggests that the overall reaction was not significantly altered by activator dosage, and that Na_2SiO_3 primarily influences the rate rather than the extent of hydration. Comparable trends have been observed in alkali-activated slag systems by Ben Haha et al. [55], where NaOH activation accelerated early hydration but did not result in a higher ultimate degree of reaction compared to Na_2SiO_3.

In contrast to silicate activation, carbonate activation led to a multi-day induction period which could be related to the early reactions between released Ca^{2+} and carbonate species, leading to the formation of metastable carbonate phases such as gaylussite ($Na_2Ca(CO_3)_2{\cdot}5H_2O$). The precipitation of these carbonate phases limits the accumulation of Ca^{2+} and OH^- in the pore solution, thereby delaying the conditions required for significant C–(A)–S–H formation. However, a review of the literature confirms that the impact of sodium carbonate on early hydration kinetics is highly system-dependent. In the hybrid system studied by García-Lodeiro et al. [5], consisting of 30 wt% Portland cement and 70 wt% fly ash, activation was carried out using either NaOH + Na_2SiO_3 or Na_2CO_3. The authors reported that Na_2CO_3 activation resulted in the early formation of gaylussite, which produced initial calorimetric peaks and higher early reaction rates than the water-hydrated system. However, the precipitation of carbonate phases temporarily reduced the alkalinity of the pore solution and delayed the precipitation of the gels compared with the NaOH + Na_2SiO_3 system. Gaylussite was detected at early ages but disappeared by 7 days, indicating its transformation as the reaction progressed. In Na_2CO_3-activated slag systems, Bernal et al. [56], reported a multi-day induction period (~62 h) associated with early formation of calcium carbonates and gaylussite, which were progressively consumed as C–A–S–H formation accelerated. In a subsequent study using a blended Na_2CO_3/Na_2SiO_3 activator, Bernal et al. [48], showed that the presence of soluble silicate shortened the induction period, highlighting the sensitivity of carbonate effects to the activator chemistry and alkalinity. In the work of Wang et al. [57], Na_2CO_3-activated slag exhibited no significant acceleration peak within the first 120 h, while the addition of CaO-rich recycled fines shortened the induction period; in that study, gaylussite was detected at early ages but largely disappeared by 28 days and was explicitly described as transient. Across these studies, gaylussite consistently appears at early ages and diminishes or disappears as hydration progresses, indicating that it mainly influences early reaction kinetics. In the present system, crystalline gaylussite was not detected within XRD at 7, 28, or 90 days; however, given its reported transient character in the literature, its short-lived formation cannot be excluded. Compared with the hybrid FA–OPC system of Garcia-Lodeiro et al. [5], the present binder contains a larger intrinsic carbonate reservoir (limestone) and a lower clinker fraction, which may contribute to differences in early-age behavior. These comparisons suggest that sodium carbonate can produce markedly different kinetic responses depending on binder chemistry, and a deeper mechanistic understanding of carbonate effects across different systems would require further targeted investigation.

Na_2SO_4 activation leads to a distinct calorimetric response compared to both silicate and carbonate activation, reflecting the role of sulfate in controlling aluminate reactions. The intensified first peak without its earlier onset (Fig. 6e) suggests that the effect of Na_2SO_4 is not primarily associated with an immediate and significant increase in pH, which would typically shorten the induction period, but rather with sulfate-mediated reaction processes. In particular, sulfate can consume dissolved Al^{3+} through ettringite formation, thereby reducing aluminate availability in the pore solution. Since aluminium species are known to adsorb on silicate surfaces [51], and reduce their dissolution rates with the magnitude of the effect linked to their concentration [52], a decrease in aluminate concentration would be expected to reduce surface passivation and thereby facilitate silicate dissolution, contributing to the observed increase in peak intensity. Further confirmation of this mechanism would require pore solution analysis in the present system.

As shown in Fig. 6g, the heat flow in the first 30 min is highly dependent on the Na_2SO_4 introduction route. The REF-CC50 paste exhibits a pronounced initial exothermic peak (≈35 mW/g), and a similar early peak is observed when Na_2SO_4 is introduced as a pre-dissolved solution (≈40 mW/g). In contrast, when $Na_2SO_4{\cdot}10H_2O$ is added as a dry solid, the initial signal is strongly reduced. For freshly prepared dry-mixed binders (cast within 24 h), the early peak decreases to ≈ 6 mW/g

at 1.5% Na_2O_{eq} and becomes net endothermic at 3.0% Na_2Oeq (minimum around −10 mW/g). This behaviour indicates that the very early signal is not controlled by hydration reactions alone. In the dry-mixing method, the solid activator must dissolve and ions must equilibrate, and these rapid physical processes (wetting/adsorption and dissolution/ion redistribution) can substantially modify the net heat flow. At higher activator content, the magnitude of this early physical contribution increases and can outweigh the early exothermic hydration signal, resulting in a net endothermic response.

After prolonged dry storage, the initial heat flow becomes very small (≈10 mW/g at 1.5% Na_2O_{eq} and close to zero at 3.0% Na_2O_{eq}). The strongly reduced initial signal suggests that the processes responsible for the early exothermic peak in the fresh pastes are less active after storage. This is consistent with pre-hydration of the dry blend during storage, likely involving partial release/redistribution of crystal water from $Na_2SO_4{\cdot}10H_2O$. Such effects can reduce the amount of "fresh" reactive surface available at the start of the test and slow the initial dissolution/precipitation reactions after water addition. At the same time, storage can also change the hydrate state of the sodium sulfate decahydrate which leads to change in its dissolution heat release. As a result, both the early exothermic contribution and the early physical contribution are reduced, and the net heat flow approaches zero in the high-dosage case where these contributions can nearly balance.

While the calorimetric analysis above focuses on identifying and assigning the main heat evolution peaks, it is also important to examine how these kinetic features relate to compressive strength development. The prolonged induction period observed for NC-1.5-P and NC-3-P, characterized by the absence of a distinct main hydration peak after the first two days, corresponds directly to the lack of measurable early strength and delayed demolding behavior. This kinetic delay in the Na_2CO_3-activated system is reflected quantitatively in the very low cumulative heat at 2 days, 50 J/g and 60 J/g for 1.5% and 3.0% Na_2O_{eq}, respectively, compared with 136.4 J/g for REF-CC50. In contrast, N$-1.5-P does not exhibit an earlier onset of the main hydration peak but shows a substantially higher peak intensity. This results in a cumulative heat of approximately 190 J/g at 2 days, which corresponds to the significantly higher 2-day strength of 18.8 MPa compared with 7.2 MPa for the REF-CC50. These observations indicate that differences in early hydration rate and reaction extent are reflected consistently in early strength development across the activator systems.

At 7 days, the overall strength ranking broadly follows the cumulative heat release, indicating that reaction extent remains a primary factor governing mechanical performance. For example, the sulfate-activated system at 1.5% Na_2O_{eq} exhibits both slightly higher cumulative heat and higher compressive strength compared with the reference, demonstrating a consistent relationship between hydration progress and strength development. Similarly, the silicate- and carbonate-activated systems show lower cumulative heat and correspondingly lower strength, suggesting reduced reaction efficiency or differences in hydrate formation.

At 7 days, NSi-1.5-P (172.3 J/g) and NSi-3-P (164 J/g) show cumulative heat values comparable to NC-3-P (170 J/g); however, their compressive strengths differ, reaching 13.6 MPa and 10.8 MPa for the silicate systems compared with 14.9 MPa for NC-3-P. This indicates that similar cumulative heat does not necessarily result in identical mechanical performance, as differences in hydrate assemblage, phase composition, and microstructural development can influence how effectively the reaction products contribute to strength.

For sodium sulfate systems dry-mixed and stored for more than 24 h, compressive strength converges to similarly low values at both dosages. In calorimetry, however, the higher dosage shows lower 7-day cumulative heat than the lower dosage. This difference must be interpreted together with the early heat flow: the higher-dosage, long-stored system exhibits an initial heat flow close to 0 mW/g, whereas the lower dosage still shows a small exothermic response. Since cumulative heat integrates the entire signal, suppression of the early exothermic contribution reduces the 7-day total heat.

The influence of activator addition method observed here for sodium sulfate-activated system differs from that reported by Fernández-Jiménez et al. [25], where slightly higher early strength was observed when sodium sulfate was incorporated as a solid in a 50% OPC–50% fly ash hybrid cement, while long-term strengths were similar. In that study, the activator is described simply as sodium sulfate without specification of hydrate form. Since hydrated salts are usually explicitly identified when used, it is likely that anhydrous Na_2SO_4 was employed. In contrast, the present study used $Na_2SO_4{\cdot}10H_2O$, which DVS measurements show can release crystalline water under typical laboratory humidity, making dry blends sensitive to storage prior to casting. Therefore, the discrepancy is attributed to differences in the hydrate form of sodium sulfate and the resulting storage sensitivity of the dry mixtures, rather than to an inherent effect of solid versus dissolved addition.

4.2. *Reaction progress and hydrate assemblage: Insights from TGA and XRD*

The evolution of bound water, portlandite, carbonate phases, and AFt/AFm assemblage provides a clear view of how each binder progresses during hydration. TGA and XRD results reveal distinct reaction pathways across the reference and activated systems, reflecting differences in both the extent and type of hydrate formation. The low bound water (BW) content of the REF-L75 system (Fig. 7) is consistent with the low clinker content of this system and the absence of pozzolanic reaction. The higher BW values of the REF-CC50 system are attributed to the pozzolanic reactivity of calcined clay. For the alkali-activated systems, the consistently high BW of the Na_2SO_4-activated binder (N$-1.5-D-24 h), especially at early age (11.8 wt% at 2 days), aligns with its higher early compressive strength (Fig. 2) and with the formation of ettringite (Fig. 9c).

The relationship between bound water content and early-age strength is not necessarily linear in blended and alkali-activated systems. In the present study, the Na_2SiO_3-activated system (NSi-1.5-P) exhibited lower bound water at 2 days than REF-CC50 (Fig. 7), while developing higher compressive strength (Fig. 2). This apparent inconsistency can be attributed to differences in hydrate chemistry and microstructural configuration rather than to the total amount of bound water alone The XRD analysis (Fig. 9b) showed that REF-CC50 contained ettringite and monocarbonate (AFt and AFm phases), while NSi-1.5-P primarily formed a sodium-substituted AFm-type phase (U-phase) (Fig. 9c). The amount of structurally bound water depends strongly on the type of hydrates present. Ettringite has the conventional composition $Ca_6Al_2(SO_4)_3(OH)_{12}{\cdot}26H_2O$, corresponding to 26 moles of structural water per formula unit [58], which is substantially higher than that of the sodium-substituted AFm-type U-phase with a structural formula of $[3Ca_2Al(OH)_6][Na(H_2O)_6(SO_4)_2{\cdot}6H_2O]$, corresponding to approximately 12 moles of structural water per formula unit [59]. Consequently, systems dominated by AFt phases may exhibit higher bound water contents even when the whole phase assemblage leads to lower strength. Similar cautions regarding direct comparison of bound water between systems with different hydrate assemblages have been reported by Ben Haha et al. [55].

Beyond BW evolution, consideration of the phase assemblage provides additional insight into the hydration mechanisms of the systems. In particular, the absence of portlandite in alkali activated systems (Fig. 8) is not due to instability, but because the clinker content (≤25%) is insufficient to sustain $Ca(OH)_2$ accumulation. Early Ca^{2+} released is rapidly incorporated into binding gels, and further strength development (e.g., ~4 MPa increment from 2 days to 28 days in N$-1.5-D-24h) is likely governed by continued gel formation and interaction between the aluminosilicate gel and SCMs, rather than portlandite-mediated reactions.

The XRD results (Fig. 9) provide further insight into the hydrate

assemblages governing the observed behavior. The persistence of monocarbonate in REF-L75 is thermodynamically expected in well-hydrated, space-available environments, where monocarbonate becomes the stable phase under excess water and limited ion-transport constraints. In REF-CC50, the coexistence of hemicarbonate and monocarbonate indicates localized carbonate limitations, likely associated with microstructural refinement during calcined-clay reaction, which reduces the availability of reactive species for carboaluminate formation. This interpretation aligns with the findings of Avet et al. [60] who showed that metakaolin contributes to extensive hydrate formation and pore refinement, thereby influencing the distribution and stability of carboaluminate phases.

For the activated systems, XRD further reveals how different activators modify hydrate assemblage and phase stability. In the Na_2SO_4-activated system, the strong and persistent ettringite reflections (Fig. 10c) indicate stable ettringite formation. The formation of ettringite is directly linked to early strength development (Fig. 2) and reduced porosity (Fig. 10), as it contributes to early solid-volume generation due to its high molar volume. This is consistent with findings by Etcheverry et al. [12] who reported similar effects in hybrid systems containing Portland cement and blast furnace slag when activated by Na_2SO_4.

In contrast to Na_2SO_4 activation, Na_2SiO_3 activation leads to a distinctly different AFm chemistry, as reflected in the XRD patterns. The U-phase observed in Na_2SiO_3 activated system was also reported in LC^3 systems containing Na_2SiO_3 activators, particularly at higher Na_2O_{eq} dosages [16], confirming its preferential formation under elevated Na^+ concentrations. Although the Na_2O_{eq} dosage was identical in the three activated systems in this study, this does not imply identical effective alkalinity (pore-solution pH and OH^- activity), which governs U-phase stability. Thermodynamic and experimental studies indicate that U-phase formation is characteristic of sodium-enriched systems under strongly alkaline conditions, with stability controlled by the alkalinity regime rather than total sodium availability alone [61]. Sodium silicate generally produces higher effective alkalinity compared to sodium sulfate or sodium carbonate, which are commonly described as mildly or weakly alkaline activators relative to silicate- or hydroxide-based systems [46,48]. As a result, even at the same Na_2O_{eq} dosage, differences in activator type can lead to substantially different pore-solution pH. Under the investigated conditions, sodium silicate is therefore the activator most capable of generating the high-alkali environment required for U-phase stabilization which explains why U-phase was observed only in the silicate-activated system despite equal Na_2O_{eq} dosages. This difference in hydrate assemblage is also reflected in the mechanical response. Despite the accelerated hydration observed in the sodium silicate system, the silicate activated binder exhibits lower strength development than the sulfate-activated system. The U-phase-dominated assemblage formed under high-alkali conditions appears less effective in contributing to mechanically efficient solid-phase development than the AFt-rich system formed in the presence of sodium sulfate. It should be noted, however, that the presence of U-phase is better interpreted as an indicator of highly alkaline conditions than as the sole and direct cause of the reduced strength. Direct comparisons of activators in white cement have shown that highly alkaline NaOH activation can result in lower strength than Na_2SO_4 activation at a comparable degree of hydration, due to differences in hydrate assemblage and pore structure development [9]. Similar trends have also been reported in hybrid fly ash systems, where higher NaOH contents were associated with loosely packed C-A-S-H-type phases, increased capillary porosity, and lower later-age strength [62]. In Portland cement systems, it has been shown that high OH^- concentrations can reduce later-age strength development, which has been attributed to faster internal drying, reduced pore saturation, and a lower degree of hydration at later ages [15]. In this context, the lower strength observed in the sodium silicate-activated system in the present study is more likely related to the influence of the high-alkali regime on hydration and microstructural development, with U-phase serving primarily as an indicator of these highly alkaline conditions.

The Na_2CO_3–activated system exhibits further deviations in phase assemblage, particularly with respect to AFt and AFm formation. As shown in Fig. 9e, neither AFt nor AFm phases were detected in the stopped Na_2CO_3-activated samples. Although previous studies on Na_2CO_3–activated hybrid binders similarly reported the absence of ettringite, they did observe AFm carbonate formation [22]. Given the known sensitivity of AFm phases to hydration stoppage procedures, this raised the question of whether these phases were absent during hydration or destabilized during sample preparation. To verify whether the missing phases in the present work were truly absent in the fresh state or had decomposed during sample hydration stoppage, additional XRD measurements were performed on fresh, un-stopped slices of the Na_2CO_3-activated paste. These in-situ measurements show clear hemicarbonate reflections, indicating that AFm-carbonate phases are present during hydration but do not remain stable after the stopping procedure (Fig. 10f). It should also be noted that AFm-carbonate phases are detectable in TGA measurements, where a weak mass-loss signal corresponding to AFm dehydration is observed (Fig. S1e). Both XRD and TGA samples were stored under identical conditions in a desiccator for 4 days up to 1 week prior to measurement; therefore, the discrepancy is not related to different storage durations. Rather, AFm phases could be poorly crystalline or semi-crystalline and may not generate sufficiently intense diffraction peaks for detection by XRD after stoppage, whereas TGA is sensitive to dehydration reactions and can detect such phases even when long-range structural order is limited. Nevertheless, the AFm-related signal in TGA is relatively weak, indicating that only minor amounts are present.

The absence of strätlingite in all of the systems despite the high reactivity of calcined clay and the absence of portlandite is consistent with Zajac et al. [63]. They reported that strätlingite formation is strongly suppressed in systems with limited calcium local availability and that, in carbonate-containing blends, silicates preferentially precipitate as low Ca/Si C–S–H rather than strätlingite. As microstructural or compositional analyses such as SEM–EDS were not performed in the present study, the Ca/Si ratio of the C–S–H cannot be directly assessed. Nevertheless, the absence of strätlingite observed here aligns with the trends reported in the literature. Similarly Kunther et al. [64] reported that in their ternary white Portland cement-metakaolin-limestone systems, strätlingite was observed to be strongly diminished when limestone was incorporated into the blend. Consistently, Zunino et al. [65] in a comprehensive review of calcined clay–limestone systems, explain that limestone limits strätlingite formation.

4.3. Porosity characteristics and their implications for strength development

This section examines how porosity quantified by different techniques evolves across the systems studied and discusses what these porosity characteristics imply for strength development. Before comparing porosity trends across systems, it is important to clarify the differences between porosity values derived from TGA and MIP. As indicated in Fig. 10, TGA derived porosities are always higher than the MIP porosities. Such a trend is expected because the mass-balance approach from TGA accounts for all water-accessible porosity, including gel-scale pores, whereas MIP does not intrude the finest pores and therefore underestimates the total porosity. Despite the difference in absolute magnitude, both methods follow the same overall pattern. When considered alongside the strength results, the largely unchanged porosity observed in the alkali-activated systems over time becomes particularly significant. In the activated systems, strength development occurs even though both MIP and TGA-derived porosities (Fig. 10 and Table S3) remain essentially stable over time. For example, the Na_2SO_4-activated system shows compressive strength increasing from 18.8 MPa at 2 d to 26.3 MPa at 90 d, while its TGA porosity remains nearly constant (47–48%). Similarly, the Na_2SiO_3 activated system increases from

10.9 MPa at 2 d to 16.2 MPa at 90 d, despite its TGA porosity staying in the narrow range of (50–51%). Such behavior has been discussed in recent literature. Zajac et al. [66] noted that higher strengths at later ages can occur even in systems with relatively high or unchanged porosities, because the decisive factor is the spatial arrangement of hydrates rather than the total void fraction. Similarly, Zajac et al. [67] emphasized that there is no single universal relationship between porosity and strength.

The limited change in CPD of alkali activated systems (Fig. 11), unlike the reference systems, suggest that activator chemistry promotes an early stabilization of the pore network, with minimal subsequent refinement during hydration. This interpretation should, however, be treated with caution, as CPD represents the most frequent pore entry size rather than the full pore connectivity, and mercury intrusion porosimetry does not fully capture gel-scale porosity.

To further examine how pore structure relates to strength development, the pore population within the predefined MIP-accessible window (50 nm to 5 μm) was partitioned into fractions finer and coarser than the CPD and compared with compressive strength. This analysis reveals pronounced differences among the activated binders. The Na_2SO_4-activated system consistently showed the highest fraction of pores finer than the CPD at all investigated ages and also developed the highest compressive strength. In contrast, the Na_2SiO_3 –activated binder showed a progressive shift toward a larger fraction of pores coarser than the CPD with curing age, indicating coarsening of the MIP-accessible pore structure. Despite this trend, strength development still occurred. The Na_2CO_3-activated binder exhibited a stable pore fraction over time and developed with limited strength development compared to the Na_2SiO_3 –activated binder. Taken together, the combined analysis of CPD, pore-size partitioning, and coarser pore fractions demonstrates that strength development in these systems does not necessarily require refinement of the coarser pore network captured by MIP.

A quantitative evaluation of the strength–porosity relationship (Tables S4–S5, Supplementary Material) further clarifies this distinction between reference and activated systems. When all mix–age combinations of the two reference binders are considered together, compressive strength shows a strong inverse correlation with both total MIP porosity and the coarse pore fraction within the 50 nm–5 μm window ($R^2 = 0.931$ and $R^2 = 0.851$, respectively). This indicates that, in the reference systems, strength development is closely associated with systematic refinement of the coarser MIP-accessible pore domain (Fig. 12). In contrast, when the activated binders are analyzed separately, the strength and (50 nm–5 μm) porosity relationship is substantially weaker ($R^2 = 0.422$), and the fraction of pores coarser than the CPD exhibits a low coefficient of determination ($R^2 = 0.337$), indicating a weak statistical relationship with strength. These results demonstrate that, while coarse pore refinement captured by MIP is an effective descriptor of strength evolution in reference binders, it does not provide a universal explanation for strength development in the activated hybrid systems. In the activated binders, strength increases occur despite minimal changes in the coarse pore fraction, indicating that the governing microstructural changes are not primarily reflected in the MIP-accessible coarse network. Instead, strength development must be interpreted together with activator-controlled hydrate assemblage and reaction progress (4.1–4.2 and 4.4), as well as the spatial organization and connectivity of hydration products at length scales not fully captured by MIP.

Complementary insight is provided by BET measurements. N_2-BET reflects surfaces accessible to nitrogen at 77 K and is commonly interpreted as indicative of gel scale surface development during hydration, whereas H_2O-BET probes narrower and more hydrophilic surface domains that are not readily accessed by nitrogen. Together, these measurements provide an indirect indication of changes in accessible surface area during hydration. Although both the Na_2SiO_3 and Na_2SO_4-activated systems exhibited similarly high, and the highest overall, H_2O-BET values among all mixtures, the Na_2SO_4-activated system developed substantially higher compressive strength than the Na_2SiO_3-activated binder. These observations indicate that a high hydrophilic surface area, as reflected by H_2O-BET, is not by itself sufficient to ensure high mechanical performance. Instead, the results suggest that strength development depends not only on surface area but also on the spatial organization and connectivity of hydration products within the microstructure which are the features that are not directly captured by BET measurements.

4.4. Integrated mechanistic interpretation of strength development

The combined mechanical, calorimetric, phase assemblage, and pore structure results demonstrate that strength development in these ultra-low-clinker hybrid binders is governed primarily by activator-controlled phase evolution and hydrate connectivity rather than by total porosity or critical pore diameter alone. Because clinker content is limited to 25 wt%, the system operates near calcium deficiency; consequently, small variations in calcium partitioning and aluminate reaction pathways strongly influence which hydrates form and whether a mechanically continuous skeleton can develop.

4.4.1. Role of sodium sulfate: Early load-bearing structure formation

Sodium sulfate activation promotes rapid and persistent ettringite (AFt) formation, as shown by XRD (Fig. 9c), together with high early bound water and intensified calorimetric peaks (Fig. 6e). Sulfate effectively incorporates dissolved aluminum into AFt, reducing aluminate availability in the pore solution and enabling continued silicate hydration (detailed explanation in 4.1). This stabilizes a crystalline aluminate-bearing phase rather than redistributing aluminum into alternative AFm structures.

Despite only limited evolution of total porosity (Fig. 10) and critical pore diameter over time (Fig. 11), the Na_2SO_4-activated system exhibits the highest early and long-term compressive strength among all activated systems and demonstrated strength development over hydration period (Fig. 2). This indicates that strength development is not driven by progressive pore refinement but by early formation of a space-filling and load-bearing AFt-supported framework. Once this framework is established, subsequent hydration primarily densifies and strengthens the existing skeleton rather than reorganizing the capillary pore network. Nevertheless, it should be noted that the long-term compressive strength remained slightly below that of the reference system which could be due to the faster internal drying, reduced pore saturation, and a somewhat lower degree of hydration at later ages due to the addition of alkali activator [14,15].

4.4.2. Role of sodium metasilicate: Gel development with modified AFm chemistry

Sodium metasilicate activation results in a distinct hydrate assemblage compared to the sulfate-activated system. XRD analysis indicates the formation of a Na-substituted AFm phase (U-phase) rather than AFt (Fig. 9d), suggesting that aluminum is preferentially incorporated into Na-bearing layered structures instead of ettringite-type frameworks. Although early hydration is accelerated (Fig. 6a) and the H_2O-BET surface area is among the highest of all systems (Fig. 14), the corresponding compressive strength remains substantially lower than that of the Na_2SO_4-activated binder. This indicates that rapid gel formation and increased surface development alone are insufficient to ensure mechanical efficiency. In this system, strength evolution appears to be governed primarily by gel densification, while the high-alkali conditions, reflected in the predominance of U-phase and the absence of a continuous AFt-type crystalline framework, appear to limit the load-bearing capacity.

4.4.3. Role of sodium carbonate: Calcium sequestration and delayed strength development

Sodium carbonate activation produces the most pronounced delay in hydration kinetics (Fig. 6c), consistent with early interaction between

calcium and carbonate species. Fresh-slice XRD confirms the presence of hemicarbonate during hydration (Fig. 9f). This suggests that calcium availability is partially redirected into carbonate-bearing phases, limiting participation of calcium into more structurally efficient hydrates like AFt phases.

The Na_2CO_3-activated system exhibits the smallest CPD among all binders (Fig. 11), yet develops the lowest compressive strength (Fig. 2). Total porosity (Fig. 10) and pore size distribution within the selected MIP window (Fig. 13) remain largely unchanged with curing time. These findings show that a smaller dominant pore entry size alone does not ensure improved mechanical performance. The combination of limited hydration progress, absence of stable AFt formation, and early calcium consumption appears to restrict development of a well-connected hydrate skeleton. In this case the phase evolution pathway does not favor formation of a mechanically efficient framework. As a result, strength development remains limited, and microstructural parameters remain largely unchanged with curing time.

4.4.4. Overall integration

Comparison of the reference and activated binders highlights two different strength-governing regimes. In the reference systems, strength development correlates with progressive porosity reduction (Fig. 10), consistent with classical cement behavior. In contrast, among the activated binders, differences in compressive strength occur within longer hydration period, despite comparable total porosity (Fig. 10) and only minor changes in CPD (Fig. 11) indicating that pore refinement alone does not explain the observed strength differences.

The distinguishing factor across the activated systems is the reaction pathway under calcium-limited conditions. Because clinker content is restricted to 25 wt%, calcium released during hydration is rapidly consumed, and no portlandite accumulation is observed (Fig. 8). Under these conditions, the activator controls how calcium and aluminum are partitioned among hydrates. This partitioning determines the dominant phase assemblage and the rate and extent of solid-phase development.

Systems in which early reactions promote formation of stable, high-solid-volume phases like Aft show more pronounced strength development. In contrast, systems in which calcium is temporarily redirected into alternative reactions or incorporated predominantly into gel phases show lower mechanical efficiency. The comparison therefore demonstrates that, in ultra-low-clinker hybrid binders, mechanical performance depends not only on porosity magnitude but also on the nature of the hydrates formed and the way solid phases develop during early hydration. Activator chemistry governs this phase evolution and thereby controls strength development beyond what can be inferred from pore structure parameters alone.

5. Conclusions

This study examined ultra-low-clinker hybrid binders activated with sodium sulfate, sodium carbonate, and sodium metasilicate, focusing on how activator type and incorporation method influence hydration, microstructure, and performance. The conclusions below synthesize the key findings and provide answers to our key research questions.

(1) **How does a low-clinker hybrid binder system (<25% clinker) perform in terms of early and long-term strength compared to reference systems, and what mechanisms govern this behavior?**

The ultra-low-clinker hybrid binder (25% Portland cement, 50% calcined clay, 25% limestone) showed that activator choice is decisive for early-age performance. Compared to the calcined clay reference, sodium sulfate activation at 1.5% Na_2O_{eq} provided the most effective early strength enhancement, increasing 2-day strength by about 160%, with only a minor reduction at 28 days. Strength development in activated samples occurred with hydration time without a corresponding strong reduction in porosity or critical pore diameter measured by MIP, indicating that the mechanisms governing strength evolution in these hybrid systems cannot be described only by pore refinement trends typically expected in blended cement systems. The results instead point to a combined effect of hydration kinetics and hydrate assemblage controlling early solid formation and mechanical performance.

(2) **What is the impact of alkali activator mixing method (dry vs. pre-dissolved) on mechanical performance?**

The impact of incorporation method strongly depended on the activator. For sodium sulfate, performance was highly sensitive to the addition protocol because $Na_2SO_4{\cdot}10H_2O$ can partially dehydrate during storage and promote partial pre-hydration of cement when dry-mixed and stored for more than 24 h, reducing available mixing water and suppressing hydration and strength. Pre-dissolution, or dry mixing followed by casting within 24 h, mitigated this issue and restored performance, with strengths very similar to those obtained under pre-dissolution conditions.

For sodium carbonate, compressive strength results showed negligible differences between pre-dissolving and dry mixing. However, the incorporation method did influence the hydration kinetics of the sodium carbonate binder, even though this did not translate into a strength difference under the studied conditions. For sodium metasilicate, only the pre-dissolved method was used in this study; therefore, a direct dry vs. pre-dissolved comparison cannot be made for that activator here.

(3) **How do Na_2SO_4, Na_2CO_3, and Na_2SiO_3 affect the hydration kinetics of ultra-low clinker calcined clay-based binders?**

Isothermal calorimetry revealed distinct activator-specific kinetic profiles. Sodium sulfate intensified the main hydration peak without earlier onset, which is interpreted as an indirect effect: rapid AFt formation binds Al^{3+}, reducing aluminate passivation on C_3S surfaces and enabling faster silicate dissolution once thresholds are reached. Sodium metasilicate accelerated hydration at low dosage but delayed peaks at higher dosage, likely due to increased solution viscosity. Sodium carbonate exhibited multi-day induction periods. Based on the calorimetric response, the prolonged induction period, and comparison with previous literature, this behavior was suggested to be associated with the possible formation of early carbonate-related metastable phases that temporarily control pore solution chemistry and delay the onset of the main hydration reaction. However, in the present study, this remains a plausible explanation rather than direct experimental confirmation.

Regarding incorporation method effects on hydration for the sodium carbonate binder, the timing of the first calorimetric peak was influenced by the method of addition (pre-dissolved or dry-mixed). However, no systematic trend was observed, and the shifts in peak timing were limited to only a few hours, which is minor compared to the overall induction period (>50 h). This indicates that, for Na_2CO_3, the addition method affects early-age kinetics but does not exert a dominant control over the overall reaction kinetics under the studied conditions.

(4) **Do these activators differ in their impact on strength development? If so, what mechanisms, such as changes in porosity or phase assemblage, explain these differences?**

Yes, the activators differed strongly in their impact on strength development. Sodium sulfate at 1.5% Na_2O_{eq} delivered the highest early strength and maintained comparatively favorable later-age performance. Sodium metasilicate promoted hydration acceleration at low dosage but did not achieve strength comparable to sodium sulfate activation, and higher dosage led to strength reduction. Sodium carbonate caused severe early retardation and reduced strengths at all studied ages, even though it produced the lowest critical pore diameter among the systems.

Phase assemblage differences support these performance

trends. XRD confirmed AFt in sulfate-activated systems, Na-AFm (U-phase) candidates in silicate-activated systems, and limited AFm phases in carbonate-activated systems, with AFm-carbonates detected in fresh Na_2CO_3 samples but not persisting after hydration stoppage. Microstructural descriptors based on porosity and surface area were not sufficient on their own to explain strength. Strength development in activated samples occurred without significant reduction in porosity or CPD measured by MIP, and coarse porosity population estimates (split at 20 nm and 50 nm thresholds) indicated minimal refinement between 2 and 90 days for activated binders. Sodium metasilicate activation produced the highest H_2O-BET values, reflecting extensive water-accessible surface development, but this did not translate into proportional strength. Together, these observations indicate that strength development is not governed by pore-scale refinement or surface area alone. Instead, mechanical performance is influenced by a combination of microstructural factors related to the nature and spatial organization of the hydration products, such as phase assemblage and solid-phase connectivity at smaller length scales that are not captured by MIP or BET. Further investigation is required to clarify the relative contribution of these factors.

This study identifies a practical dosage for sodium sulfate activation (1.5% Na_2O_{eq}) that delivers substantial early strength gains while limiting long-term disadvantages, provided mixing protocols prevent dehydration of $Na_2SO_4{\cdot}10H_2O$ and prehydration of the cement clinker. Under the specific conditions evaluated here, the results underline the limitations of sodium metasilicate and sodium carbonate in very low-calcium systems. Overall, activator choice and incorporation method emerge as decisive factors for performance. These findings contribute to a clearer understanding of how chemical interactions govern hydration and mechanical behavior in hybrid systems.

Limitations and future research directions

Although a multi-technique approach was used in this research, some complementary techniques could be included in future investigations to further refine the mechanistic interpretation. For example, techniques such as ^1H NMR relaxometry could improve characterization of gel-scale porosity, pore solution extraction could provide direct information on ionic evolution during hydration, in situ XRD or FTIR could help identify transient early-age carbonate phases, and SEM–EDS analysis could provide deeper insight into gel chemistry and SCM reaction degree. In addition, validation at the concrete scale would be valuable to assess practical performance, including rheology, durability-related aspects, and aggregate-binder interactions.

The activation levels and performance trends identified in this study apply to the investigated material system and experimental framework. Because hydration kinetics, phase assemblage development, microstructure, and strength evolution in hybrid binders depend on raw material characteristics and processing conditions, application to other binder compositions would require verification and potential re-evaluation of activator type, dosage, and resulting performance.

CRediT authorship contribution statement

Hania Miraki: Writing – review & editing, Writing – original draft, Visualization, Methodology, Investigation, Formal analysis, Data curation, Conceptualization. **Maciej Zajac:** Writing – review & editing, Supervision, Resources, Project administration, Conceptualization. **Mohsen Ben Haha:** Supervision, Project administration, Conceptualization. **Arnaud Muller:** Writing – review & editing, Formal analysis. **Klaartje de Weerdt:** Writing – review & editing, Formal analysis. **Ravi Patel:** Writing – review & editing, Formal analysis. **Frank Dehn:** Supervision, Conceptualization.

Declaration of Generative AI and AI-assisted technologies in the writing process

During the preparation of this work the authors used Microsoft Copilot to assist with language editing and sentence refinement. After using this tool, the authors reviewed and edited the content as needed and take full responsibility for the content of the published article.

Declaration of Competing Interest

The authors declare that they have no known competing financial interests or personal relationships that could have appeared to influence the work reported in this paper.

Acknowledgements

We gratefully acknowledge the fruitful discussions with Dr. Patrick Ullrich and Dr. Ana Costa. The contribution and involvement of colleagues of the Analytic Center (ANC) in Heidelberg Materials Global R&D are highly appreciated.

Appendix A. Supporting information

Supplementary data associated with this article can be found in the online version at doi:10.1016/j.conbuildmat.2026.146166.

Data Availability

Data will be made available on request.

References

[1] K. Scrivener, M. Ben Haha, P. Juilland, C. Levy, Research needs for cementitious building materials with focus on Europe, RILEM Tech. Lett. 7 (2023), https://doi.org/10.21809/rilemtechlett.2022.165.
[2] D. Ravikumar, S. Peethamparan, N. Neithalath, Structure and strength of NaOH activated concretes containing fly ash or GGBFS as the sole binder, Cem. Concr. Compos 32 (2010) 399–410, https://doi.org/10.1016/j.cemconcomp.2010.03.007.
[3] A. Fernández-Jiménez, A. Palomo, M. Criado, Microstructure development of alkali-activated fly ash cement: a descriptive model, Cem. Concr. Res. 35 (2005) 1204–1209, https://doi.org/10.1016/j.cemconres.2004.08.021.
[4] L. Xue, Z. Zhang, H. Wang, Early hydration kinetics and microstructure development of hybrid alkali activated cements (HAACs) at room temperature, Cem. Concr. Compos. 123 (2021) 104200, https://doi.org/10.1016/j.cemconcomp.2021.104200.
[5] I. Garcia-Lodeiro, A. Fernandez-Jimenez, A. Palomo, Hydration kinetics in hybrid binders: early reaction stages, Cem. Concr. Compos. 39 (2013) 82–92, https://doi.org/10.1016/j.cemconcomp.2013.03.025.
[6] J.L. Provis, Alkali-activated materials, Cem. Concr. Res. 114 (2018) 40–48, https://doi.org/10.1016/j.cemconres.2017.02.009.
[7] A. Kumar, G. Sant, C. Patapy, C. Gianocca, K.L. Scrivener, The influence of sodium and potassium hydroxide on alite hydration: experiments and simulations, Cem. Concr. Res. 42 (2012) 1513–1523, https://doi.org/10.1016/j.cemconres.2012.07.003.
[8] B. Mota, T. Matschei, K. Scrivener, The influence of sodium salts and gypsum on alite hydration, Cem. Concr. Res. 75 (2015) 53–65, https://doi.org/10.1016/j.cemconres.2015.04.015.
[9] B. Mota, T. Matschei, K. Scrivener, Impact of NaOH and Na2SO4 on the kinetics and microstructural development of white cement hydration, Cem. Concr. Res. 108 (2018) 172–185, https://doi.org/10.1016/j.cemconres.2018.03.017.
[10] M. Gassó, 2015, Impact of alkali salts on the kinetics and microstructural development of cementitious systems.
[11] J. Fu, A.M. Jones, M.W. Bligh, C. Holt, L.M. Keyte, F. Moghaddam, S.J. Foster, T. D. Waite, Mechanisms of enhancement in early hydration by sodium sulfate in a slag-cement blend – Insights from pore solution chemistry, Cem. Concr. Res. 135 (2020) 106110, https://doi.org/10.1016/j.cemconres.2020.106110.
[12] J.M. Etcheverry, Y.A. Villagran-Zaccardi, P. Van Den Heede, V. Hallet, N. De Belie, Effect of sodium sulfate activation on the early age behaviour and microstructure development of hybrid cementitious systems containing Portland cement, and blast furnace slag, Cem. Concr. Compos 141 (2023) 105101, https://doi.org/10.1016/j.cemconcomp.2023.105101.
[13] J.M. Etcheverry, Z. Yue, S. Krishnan, Y.A. Villagran-Zaccardi, P. Van Den Heede, Y. Dhandapani, S.A. Bernal, N. De Belie, Phase evolution of hybrid alkali sulfate-activated ground-granulated blast furnace slag cements, ACS Sustain. Chem. Eng. 11 (2023) 17519–17531, https://doi.org/10.1021/acssuschemeng.3c05937.

[14] W. Hanpongpun, K. Scrivener, in: F. Martirena, A. Favier, K. Scrivener (Eds.), The Effect of Alkali on the Properties of Limestone Calcined Clay Cement (LC3), Calcined Clays for Sustainable Concrete, Springer Netherlands, Dordrecht, 2018, pp. 200–204.

[15] M. Zhang, F. Zunino, L. Yang, F. Wang, K. Scrivener, Understanding the negative effects of alkalis on long-term strength of Portland cement, Cem. Concr. Res. 174 (2023) 107348, https://doi.org/10.1016/j.cemconres.2023.107348.

[16] X. Dai, M. Yio, H. Wu, S.B. Lopez, C. Cheeseman, H.S. Wong, Enhancing the rheology, reaction kinetics and early-age strength of limestone calcined clay cement (LC3) with sodium silicate addition, Cem. Concr. Res. 198 (2025) 107997, https://doi.org/10.1016/j.cemconres.2025.107997.

[17] J. Sun, F. Zunino, K. Scrivener, Hydration and phase assemblage of limestone calcined clay cements (LC3) with clinker content below 50, Cem. Concr. Res. 177 (2024) 107417, https://doi.org/10.1016/j.cemconres.2023.107417.

[18] F. Zunino, K. Scrivener, Hydration and strength development of low-clinker (<50%) factor limestone calcined clay cements (LC3): a comparative study with natural pozzolans, Constr. Build. Mater. 499 (2025) 144075, https://doi.org/10.1016/j.conbuildmat.2025.144075.

[19] ASTM C618-22: Specification for Coal Fly Ash and Raw or Calcined Natural Pozzolan for Use in Concrete, ⟨http://www.astm.org/cgi-bin/resolver.cgi?C618-22⟩.

[20] I. Garcia-Lodeiro, S. Donatello, A. Fernández-Jiménez, Á. Palomo, Hydration of hybrid alkaline cement containing a very large proportion of fly ash: a descriptive model, Materials 9 (2016) 605, https://doi.org/10.3390/ma9070605.

[21] S. Donatello, A. Fernández-Jimenez, A. Palomo, Very high volume fly ash cements. early age hydration study using Na $_2$ SO $_4$ as an activator, J. Am. Ceram. Soc. 96 (2013) 900–906, https://doi.org/10.1111/jace.12178.

[22] S. Alahrache, F. Winnefeld, J.-B. Champenois, F. Hesselbarth, B. Lothenbach, Chemical activation of hybrid binders based on siliceous fly ash and Portland cement, Cem. Concr. Compos 66 (2016) 10–23, https://doi.org/10.1016/j.cemconcomp.2015.11.003.

[23] A.C. Barboza-Chavez, L.Y. Gómez-Zamorano, J.L. Acevedo-Dávila, Synthesis and characterization of a hybrid cement based on fly ash, metakaolin and portland cement clinker, Materials 13 (2020) 1084, https://doi.org/10.3390/ma13051084.

[24] S. Joseph, R. Snellings, Ö. Cizer, Activation of Portland cement blended with high volume of fly ash using Na2SO4, Cem. Concr. Compos 104 (2019) 103417, https://doi.org/10.1016/j.cemconcomp.2019.103417.

[25] A. Fernández-Jiménez, I. Garcia-Lodeiro, O. Maltseva, A. Palomo, Hydration mechanisms of hybrid cements as a function of the way of addition of chemicals, J. Am. Ceram. Soc. 102 (2019) 427–436, https://doi.org/10.1111/jace.15939.

[26] M. Antoni, J. Rossen, F. Martirena, K. Scrivener, Cement substitution by a combination of metakaolin and limestone, Cem. Concr. Res. 42 (2012) 1579–1589, https://doi.org/10.1016/j.cemconres.2012.09.006.

[27] K. Scrivener, F. Avet, H. Maraghechi, F. Zunino, J. Ston, W. Hanpongpun, A. Favier, Impacting factors and properties of limestone calcined clay cements (LC^3), Green. Mater. 7 (2019) 3–14, https://doi.org/10.1680/jgrma.18.00029.

[28] V.M.E. Lima, P.A. Basto, M.A. Henrique, Y. M. B. Almeida, A.A. De Melo Neto, Optimizing the concentration of Na2O in alkaline activators to improve mechanical properties and reduce costs and CO2 emissions in alkali-activated mixtures, Constr. Build. Mater. 344 (2022) 128185, https://doi.org/10.1016/j.conbuildmat.2022.128185.

[29] F. Zunino, K. Scrivener, The reaction between metakaolin and limestone and its effect in porosity refinement and mechanical properties, Cem. Concr. Res. 140 (2021) 106307, https://doi.org/10.1016/j.cemconres.2020.106307.

[30] European Committee for Standardization: EN 196-1: Methods of testing cement – Part 1: Determination of strength, 2016.

[31] S. Adu-Amankwah, M. Zajac, P. Hou, L. Black, Impact of hydration stoppage on quantification of the GGBS content in ternary limestone cements using the PONKCS method, Mater. Struct. 56 (2023) 113, https://doi.org/10.1617/s11527-023-02198-6.

[32] K. Scrivener, R. Snellings, B. Lothenbach (Eds.), A Practical Guide to Microstructural Analysis of Cementitious Materials, CRC Press, 2018.

[33] S. Adu-Amankwah, L. Black, J. Skocek, M. Ben Haha, M. Zajac, Effect of sulfate additions on hydration and performance of ternary slag-limestone composite cements, Constr. Build. Mater. 164 (2018) 451–462, https://doi.org/10.1016/j.conbuildmat.2017.12.165.

[34] Studies of the Physical Properties of Hardened Portland Cement Paste, Acids J. Proc. 43 (1946), https://doi.org/10.14359/15302.

[35] X. Feng, E.J. Garboczi, D.P. Bentz, P.E. Stutzman, T.O. Mason, Estimation of the degree of hydration of blended cement pastes by a scanning electron microscope point-counting procedure, Cem. Concr. Res. 34 (2004) 1787–1793, https://doi.org/10.1016/j.cemconres.2004.01.014.

[36] H. Ma, Mercury intrusion porosimetry in concrete technology: tips in measurement, pore structure parameter acquisition and application, J. Porous Mater. 21 (2014) 207–215, https://doi.org/10.1007/s10934-013-9765-4.

[37] C. Gallé, Effect of drying on cement-based materials pore structure as identified by mercury intrusion porosimetry, Cem. Concr. Res. 31 (2001) 1467–1477, https://doi.org/10.1016/S0008-8846(01)00594-4.

[38] A.C.A. Muller, K.L. Scrivener, A reassessment of mercury intrusion porosimetry by comparison with ^{1}H NMR relaxometry, Cem. Concr. Res. 100 (2017) 350–360, https://doi.org/10.1016/j.cemconres.2017.05.024.

[39] A. Aili, I. Maruyama, Review of several experimental methods for characterization of micro- and nano-scale pores in cement-based material, Int. J. Concr. Struct. Mater. 14 (2020) 55, https://doi.org/10.1186/s40069-020-00431-y.

[40] N. De Belie, J. Kratky, S. Van Vlierberghe, Influence of pozzolans and slag on the microstructure of partially carbonated cement paste by means of water vapour and nitrogen sorption experiments and BET calculations, Cem. Concr. Res. 40 (2010) 1723–1733, https://doi.org/10.1016/j.cemconres.2010.08.014.

[41] F. Rouquérol, J. Rouquerol, K.S.W. Sing, Adsorption by powders and porous solids: principles, methodology, and applications, Academic Press, San Diego, 1999.

[42] R. Kurihara, I. Maruyama, Surface area development of Portland cement paste during hydration: direct comparison with ^{1}H NMR relaxometry and water vapor/nitrogen sorption, Cem. Concr. Res. 157 (2022) 106805, https://doi.org/10.1016/j.cemconres.2022.106805.

[43] M. Thommes, K. Kaneko, A.V. Neimark, J.P. Olivier, F. Rodriguez-Reinoso, J. Rouquerol, K.S.W. Sing, Physisorption of gases, with special reference to the evaluation of surface area and pore size distribution (IUPAC Technical Report), Pure Appl. Chem. 87 (2015) 1051–1069, https://doi.org/10.1515/pac-2014-1117.

[44] P.T. Durdziński, M. Ben Haha, M. Zajac, K.L. Scrivener, Phase assemblage of composite cements, Cem. Concr. Res. 99 (2017) 172–182, https://doi.org/10.1016/j.cemconres.2017.05.009.

[45] F. Avet, K. Scrivener, Investigation of the calcined kaolinite content on the hydration of limestone calcined clay cement (LC3), Cem. Concr. Res. 107 (2018) 124–135, https://doi.org/10.1016/j.cemconres.2018.02.016.

[46] W. Valencia-Saavedra, R. Robayo-Salazar, R. Mejía De Gutiérrez, Alkali-activated hybrid cements based on fly ash and construction and demolition wastes using sodium sulfate and sodium carbonate, Molecules 26 (2021) 7572, https://doi.org/10.3390/molecules26247572.

[47] J. He, S. Yu, G. Sang, J. He, J. Wang, Z. Chen, Properties of alkali-activated slag cement activated by weakly alkaline activator, Materials 16 (2023) 3871, https://doi.org/10.3390/ma16103871.

[48] S.A. Bernal, R.S. Nicolas, J.L. Provis, J.S.J. Van Deventer, Alkali-activated slag cements produced with a blended sodium carbonate/sodium silicate activator, Adv. Cem. Res. (2015) 1–12, https://doi.org/10.1680/adcr.15.00013.

[49] A. Palomo, P. Monteiro, P. Martauz, V. Bilek, A. Fernandez-Jimenez, Hybrid binders: a journey from the past to a sustainable future (opus caementicium futurum), Cem. Concr. Res. 124 (2019) 105829, https://doi.org/10.1016/j.cemconres.2019.105829.

[50] P. Suraneni, R.J. Flatt, Use of micro-reactors to obtain new insights into the factors influencing tricalcium silicate dissolution, Cem. Concr. Res. 78 (2015) 208–215, https://doi.org/10.1016/j.cemconres.2015.07.011.

[51] E. Pustovgar, R.K. Mishra, M. Palacios, J.-B. d'Espinose De Lacaillerie, T. Matschei, A.S. Andreev, H. Heinz, R. Verel, R.J. Flatt, Influence of aluminates on the hydration kinetics of tricalcium silicate, Cem. Concr. Res. 100 (2017) 245–262, https://doi.org/10.1016/j.cemconres.2017.06.006.

[52] M. Bagheri, B. Lothenbach, M. Shakoorioskooie, K. Scrivener, Effect of different ions on dissolution rates of silica and feldspars at high pH, Cem. Concr. Res. 152 (2022) 106644, https://doi.org/10.1016/j.cemconres.2021.106644.

[53] M. Zajac, J. Skocek, B. Lothenbach, B.H. Mohsen, Late hydration kinetics: Indications from thermodynamic analysis of pore solution data, Cem. Concr. Res. 129 (2020) 105975, https://doi.org/10.1016/j.cemconres.2020.105975.

[54] M.J. De Hita, M. Criado, Influence of the fly ash content on the fresh and hardened properties of alkali-activated slag pastes with admixtures, Materials 15 (2022) 992, https://doi.org/10.3390/ma15030992.

[55] M. Ben Haha, G. Le Saout, F. Winnefeld, B. Lothenbach, Influence of activator type on hydration kinetics, hydrate assemblage and microstructural development of alkali activated blast-furnace slags, Cem. Concr. Res. 41 (2011) 301–310, https://doi.org/10.1016/j.cemconres.2010.11.016.

[56] S.A. Bernal, J.L. Provis, R.J. Myers, R. San Nicolas, J.S.J. Van Deventer, Role of carbonates in the chemical evolution of sodium carbonate-activated slag binders, Mater. Struct. 48 (2015) 517–529, https://doi.org/10.1617/s11527-014-0412-6.

[57] H. Wang, L. Wang, Y. Xu, K. Cao, Y. Ge, X. Wang, Q. Li, Accelerating the reaction kinetics of Na2CO3-activated slag mortars by calcined recycled concrete fines, Materials 15 (2022) 5375, https://doi.org/10.3390/ma15155375.

[58] P.K. Sarkar, N. Mitra, D. Prasad, Molecular level deformation mechanism of ettringite, Cem. Concr. Res. 124 (2019) 105836, https://doi.org/10.1016/j.cemconres.2019.105836.

[59] D. Urushihara, T. Asaka, M. Harada, S. Kondo, M. Nakayama, M. Ogino, E. Owaki, K. Fukuda, Synthesis and structural characterization of U-phase, [3Ca2Al(OH)6][Na(H2O)6(SO4)2·6H2O] layered double hydroxide, J. Solid State Chem. 306 (2022) 122730, https://doi.org/10.1016/j.jssc.2021.122730.

[60] F. Avet, X. Li, K. Scrivener, Determination of the amount of reacted metakaolin in calcined clay blends, Cem. Concr. Res. 106 (2018) 40–48, https://doi.org/10.1016/j.cemconres.2018.01.009.

[61] M. Collin, D.P. Prentice, R.A. Arnold, K. Ellison, M. Balonis, D. Simonetti, G. N. Sant, Solubility behavior and thermodynamic modeling of sodium monosulfoaluminate ("U-phase") in cementitious systems, J. Am. Ceram. Soc. 106 (2023) 6330–6341, https://doi.org/10.1111/jace.19257.

[62] M.R. Ahmad, S. Medepalli, T. Wang, J.-G. Dai, Y. Zheng, T. Ishida, Effect of alkali-hydroxide on hydration kinetics and microstructure of high-volume fly ash blended cement pastes, Cem. Concr. Res. 185 (2024) 107641, https://doi.org/10.1016/j.cemconres.2024.107641.

[63] M. Zajac, P. Durdzinski, C. Stabler, J. Skocek, D. Nied, M. Ben Haha, Influence of calcium and magnesium carbonates on hydration kinetics, hydrate assemblage and microstructural development of metakaolin containing composite cements, Cem. Concr. Res. 106 (2018) 91–102, https://doi.org/10.1016/j.cemconres.2018.01.008.

[64] W. Kunther, Z. Dai, J. Skibsted, Thermodynamic modeling of hydrated white Portland cement–metakaolin–limestone blends utilizing hydration kinetics from 29Si MAS NMR spectroscopy, Cem. Concr. Res. 86 (2016) 29–41, https://doi.org/10.1016/j.cemconres.2016.04.012.

[65] F. Zunino, Y. Dhandapani, M. Ben Haha, J. Skibsted, S. Joseph, S. Krishnan, A. Parashar, M.C.G. Juenger, T. Hanein, S.A. Bernal, K.L. Scrivener, F. Avet, Hydration and mixture design of calcined clay blended cements: review by the RILEM TC 282-CCL, Mater. Struct. 55 (2022) 234, https://doi.org/10.1617/s11527-022-02060-1.

[66] M. Zajac, J. Skocek, S. Adu-Amankwah, L. Black, M. Ben Haha, Impact of microstructure on the performance of composite cements: why higher total porosity can result in higher strength, Cem. Concr. Compos. 90 (2018) 178–192, https://doi.org/10.1016/j.cemconcomp.2018.03.023.

[67] M. Zajac, P. Durdzinski, Z. Giergiczny, M. Ben Haha, New insights into the role of space on the microstructure and the development of strength of multicomponent cements, Cem. Concr. Compos. 121 (2021) 104070, https://doi.org/10.1016/j.cemconcomp.2021.104070.